*Mineralia Slovaca, Web ISSN 1338-3523, ISSN 0369-2086, https://doi.org/10.56623/ms.2025.57.1.2*
*57, 1 (2025), 5 – 38, © Authors 2025. CC BY 4.0*

# Geological setting and origin of Blue Cave with blue and green carbonate speleothems (Central Slovakia)

JURAJ LITTVA*[1], PAVEL BELLA[1, 2], ĽUDOVÍT GAÁL[1], and PAVEL HERICH[1, 3]

[1] State Nature Conservancy of the Slovak Republic, Slovak Caves Administration, Hodžova 11, 031 01 Liptovský Mikuláš, Slovak Republic
[2] Department of Geography, Faculty of Education, Catholic University in Ružomberok, Hrabovská cesta 1, 031 04 Ružomberok, Slovak Republic
[3] Department of Physical Geography and Geoecology, Faculty of Natural Sciences, Comenius University in Bratislava, Mlynská dolina, Ilkovičova 6, 842 15 Bratislava 4, Slovak Republic
*Corresponding author: juraj.littva@ssj.sk, https://orcid.org/0000-0002-5674-2447

**Abstract:** Blue to green carbonate speleothems are a principal feature of Blue Cave, located in the northeastern part of the Nízke Tatry Mountains. The copper, colouring the speleothems, was thought to originate from the Permian volcanics neighbouring the Middle Triassic carbonates hosting the cave. Tracing sparse mentions about the Pb-Zn-(Cu) ores in the carbonates, we identified previously overlooked studies, that studied of the mineralisation in surprising detail. Based on the data from these works, remapping of the area, and by examining the geology and geomorphology of the Blue Cave, we conclude the following. 1) The Hronic Unit near the Blue Cave forms two nappes, and the carbonates hosting the cave are involved in the structurally imbricated zone at the top of the lower nappe. 2) The imbricated thrusts predispose the Pb-Zn-(Cu) sulphide mineralisation in the carbonates, while secondary azurite and malachite follow younger NE-SW and NW-SE fractures. 3) This mineralisation, rather than the volcanics, provided copper for the coloured speleothems, formed along NW-SE fractures. 4) The dissolution of carbonates by the sulphide oxidation might have created the precursor porosity for later cave formation. 5) The Blue Cave formed in three stages. In Stage I – likely in the Middle Pleistocene – the cave formed below the water table, underneath the stream terrace levelled by the surface stream. During the later valley incision and formation of lower-lying stream terraces in Stage II, the cave was modified by episodic floodwaters. As they bear floodmarks, the coloured speleothems formed mostly during this stage. The bedded and fractured bedrock that predisposed the solution also contributed to the cave's remodelling by collapse during Stage III.

**Key words:** Hronic Unit, Pb-Zn ores, copper minerals, blue and green speleothems, speleogenesis, phreatic morphologies

**Graphical abstract**

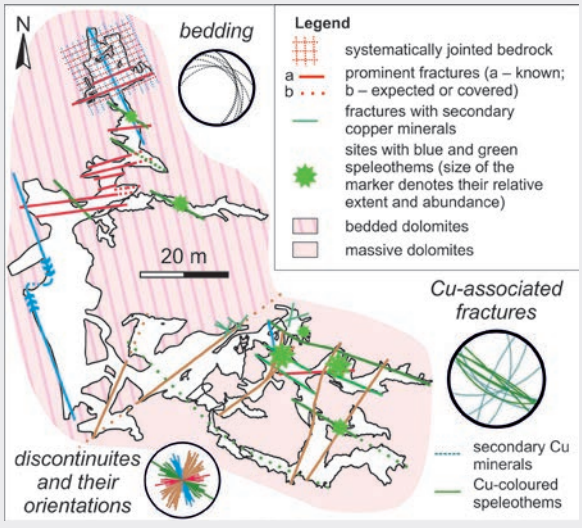


**Highlights**

- The Hronic Unit in the study area is formed by two nappes with the tectonically imbricated zone in the upper part of the lower nappe instead of three nappes originally interpreted by previous research.
- Copper, causing the colour of the cave's speleothems, is derived from the Pb-Zn-(Cu) ores in the carbonates that host the cave, not nearby basalts as previously thought.
- Malachite and azurite occurrences were discovered in the cave's host rock.
- The sulphuric acid from the oxidised sulphide ores did not form the cave, but it might have enhanced the porosity of the host rock, facilitating later karstification.
- The cave is genetically related to the levelling of the stream terrace above the cave, probably during the Middle Pleistocene, and subsequent periodical valley incision.

## Introduction

The Blue Cave (Modrá jaskyňa in Slovak), discovered near the Malužiná village in 2016 (Šmoll, 2017), is so far the only cave in the territory of Slovakia with the reported extensive occurrence of blue and green speleothems. The cave is located in northern Slovakia on the northeastern slopes of the Nízke Tatry Mountains (Fig. 1A), on the left (western) side of the valley cut by the Boca Stream. The cave entrances lie at altitudes of 752 and 767 m a.s.l.

(Pristašová, 2024), near the confluence of Boca Stream with its right tributary, the Malužiná Stream. The cave was discovered by G. Majerníčková, J. Šmoll, and M. Šušeľ, and its currently known passages reach a length of 657 m and a vertical span of 25 m (Šmoll, 2017).

Orvošová et al. (2016) used geochemical and mineralogical methods to determine copper as a predominant chromophore colouring the speleothems, although elevated amounts of zinc, barium, and iron were also detected. These elements were associated with the weathering of the Cu-Zn-Fe mineralisation in the cave's proximity. The nearby Permian volcanics containing barite-sulphide ore veinlets were considered as a likely source (Orvošová et al., 2016). However, the evidence from other research works suggests the possibility of a different copper source.

Approximately 1.5 km to the northwest of the cave, in the so-called Olovienka (approximate translation – 'Leadeling') Ravine, abandoned mines have been excavated in the same carbonate rock formation that hosts the Blue Cave. Sparse mentions in literature (e.g. Chovan et al., 1996; Biely et al., 1997, p. 186) claimed that these works exploited lead-zinc sulphide mineralisation, interpreted as metasomatic-hydrothermal in origin. This prompted further research, during which we discovered several unpublished technical reports archived in the Archive of the State Geological Institute of Dionýz Štúr (Kantor, 1957; Hanáček, 1963; Biely, 1964; Ivanov et al., 1965) and one conference paper (Kantor, 1977). These reports present comprehensive results from mineralogical and geochemical investigations conducted not only near the mines but also in the wider area, including the rocks adjacent to the Blue Cave. The data from the reports provide new perspectives on potential copper sources, prompting the reassessment of the proposition of Orvošová et al. (2016) that copper is derived from the weathering of the Permian volcanics.

Besides the presence of the uniquely-coloured carbonate speleothems, the Blue Cave could be potentially significant from a geomorphological point of view. The carbonate-hosted lead and zinc sulphide ores are associated with caves that were formed by sulphuric acid and exhibit specific morphological and mineralogical features resulting from this process (see De Waele et al., 2024 and references within). Indeed, some of the rediscovered works (Hanáček, 1963; Biely, 1964; Ivanov et al., 1965) reported the presence of sulphide minerals very close to the cave. On the other hand, the cave's position immediately downstream from the non-karstic area suggests that the cave was formed primarily by waters from the surface stream. Therefore, a study of the cave's morphology is necessary to understand which processes formed the Blue Cave.

Additional geological research of the cave was done primarily to (1) understand the characteristics of the host rock and (2) find out how the presence of fractures predisposed the distribution of the cave passages and blue and green speleothems. In addition, the study of the geological structures in the cave could also contribute to the understanding of the geology in the regional context. The region near the Blue Cave is traditionally considered one of the 'key areas' for understanding the geology of the entire Western Carpathians (Zoubek, 1952). An important tectonic contact between three high-order geological units (Tatric, Veporic, and Hronic Units) is located to the south of the cave (Fig. 1B). Hence, we will provide a brief description of the geological setting.

## Geological setting

The Čertovica thrust zone, separating the two Western Carpathian main thick-skinned geological units (Tatric and Veporic), is exposed southward from the Blue Cave (Fig. 1B). To the north, this thrust zone is overlain by a thin-skinned nappe stack of the Hronic Unit (Fig. 1B). The Hronic rocks are composed primarily of the Upper Paleozoic siliciclastic, volcaniclastic, and volcanic rocks, as well as the Mesozoic siliciclastic and carbonate formations (Biely et al., 1992; Appendix 1 in Tulis & Novotný, 1998). The Middle to Upper Triassic Hronic carbonates cropping out in the area can be assigned to two distinct facial sequences – Biely Váh Basin and Čierny Váh Platform sequence (*sensu* Havrila, 2011). The former one is a deep-water sequence occurring in the uppermost tectonic unit, while the latter one represents a shallow-water sequence present in the lower tectonic units (Fig. 1C; Biely et al., 1992, 1997; Havrila, 2011). The shallow-water Triassic carbonates that host the cave are poorly understood and lack a formal stratigraphic name; accordingly, we denote them as 'Čierny Váh carbonates'.

The tectonic structure of the Hronic Unit near the cave is complex, due to the tectonic disruption of its internal structure during multi-stage deformation. Thrusting with a general top-to-the-northwest sense of movement occurred during the Cretaceous nappe stacking (Biely, 1963; Kováč & Filo, 1992; Biely et al., 1997, p. 147–149; Kováč & Havrila, 1998). Subsequent post-Cretaceous deformation stages involved the rejuvenation and oversteepening of the thrust planes, including the dissection of the nappe stack by steep parallel and cross-cutting faults (Biely et al., 1997, p. 147–149; Tulis & Novotný, 1998, p. 70–71; Olšavský, 2008, p. 168–173). Two ore prospecting boreholes (Biely, 1964) named Ma-1 (165 m deep) and Ma-2 (145 m deep) were drilled near the cave (Figs. 1C, 2A–C, and 3). In both of them, tectonically perturbed rocks were observed underneath the fluvial sediments. In the borehole Ma-1, Biely (1964) described several repetitions of the Lower Triassic siliciclastics and Middle Triassic carbonates (Fig. 3), indicative of their intense tectonic reworking. In the

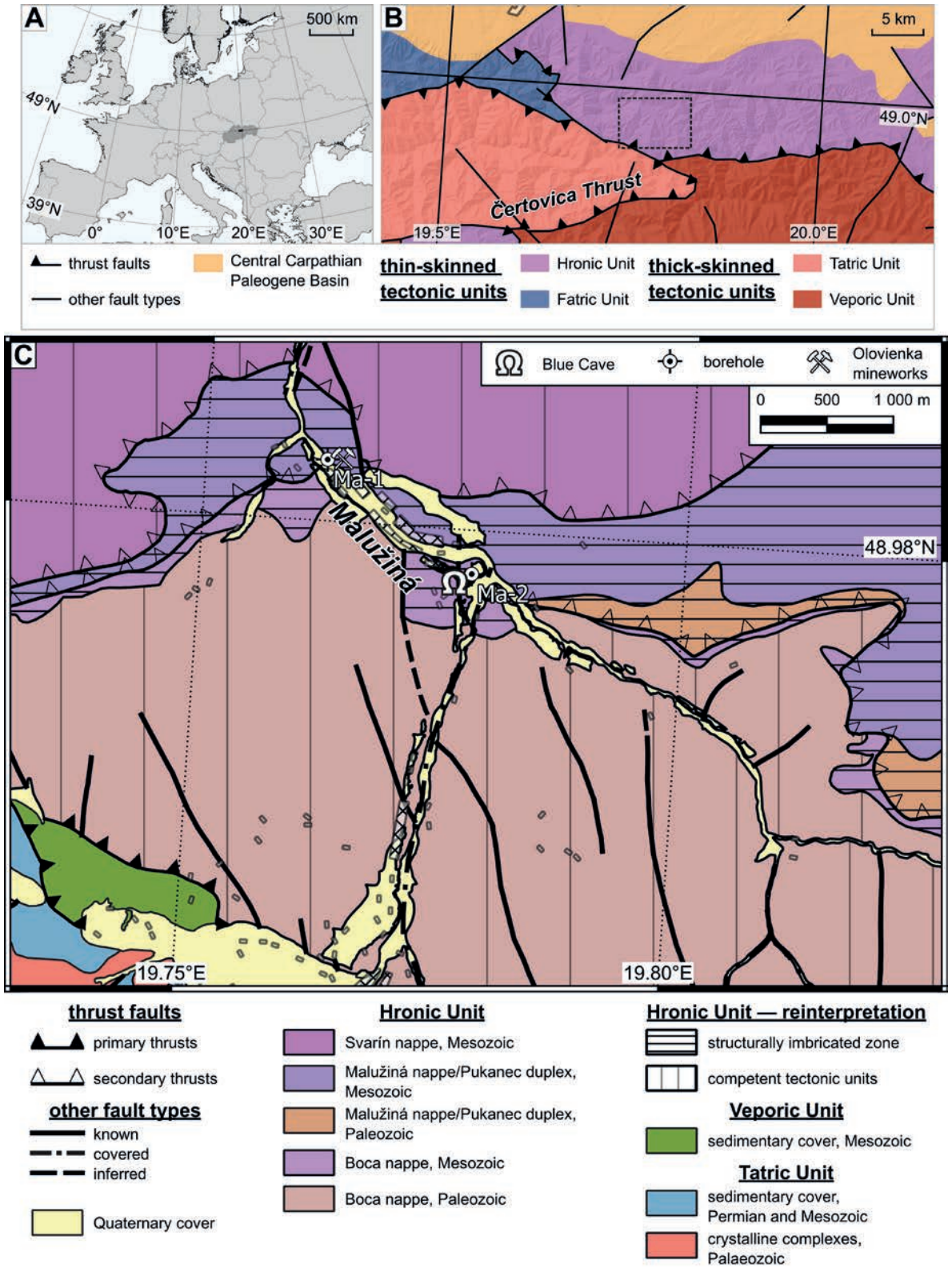


**Fig. 1.** Location and geological setting of the Blue Cave. **A** – Location of the study area shown on a map of Europe as a black rectangle. **B** – Structural sketch depicting the main tectonic units in the broader area near the Blue Cave (modified from Lexa et al., 2000), the dashed rectangle denotes the extent of figure C. **C** – Tectonic map (simplified from the original map of Biely et al., 1992) depicting main tectonic units in the vicinity of the Blue Cave according to the interpretation of Biely (1997) and our reinterpretation; the extent of Quaternary fluvial and slope sediments is based on the mapping results from this study.

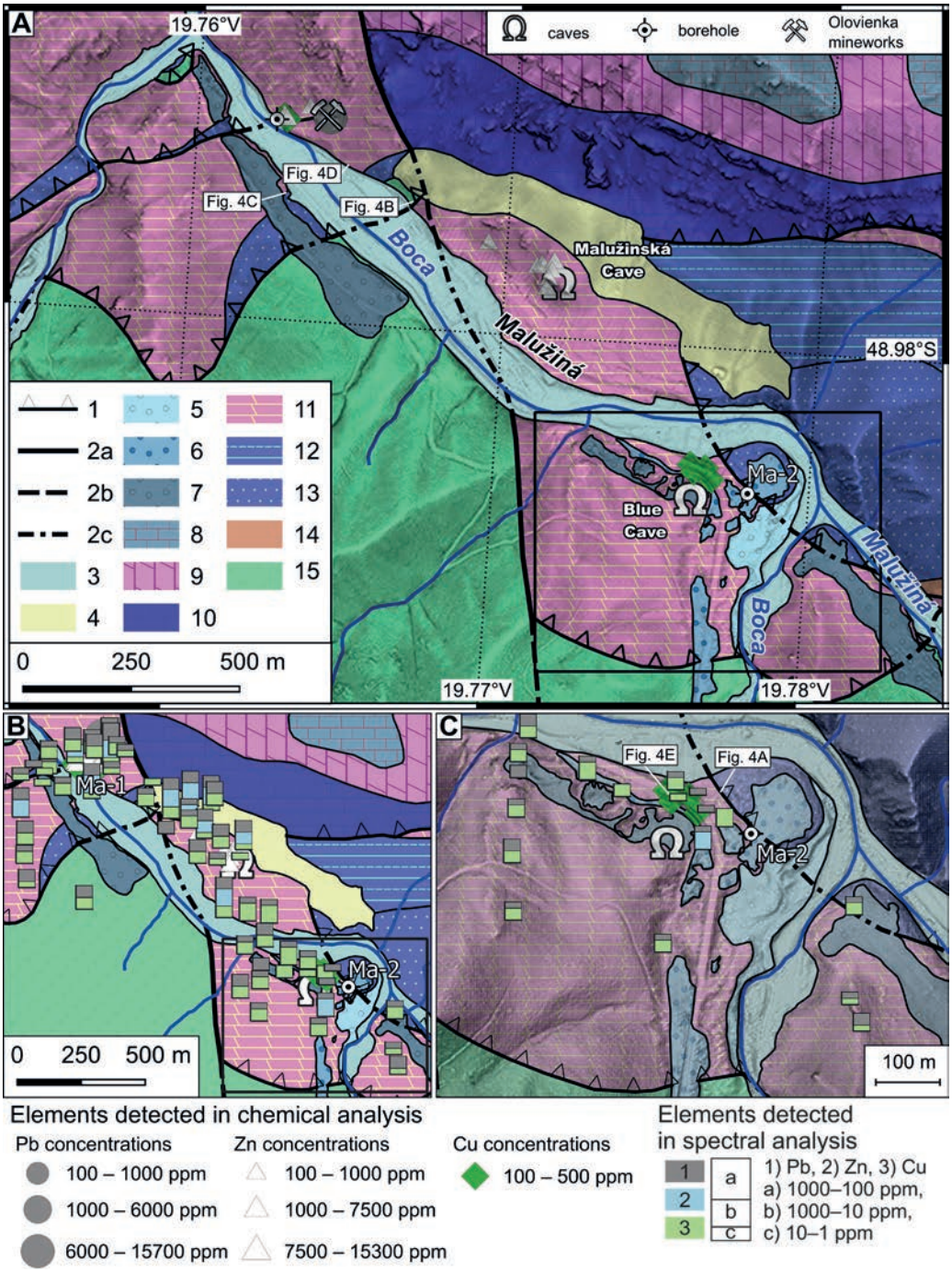


**Fig. 2.** Geology of the study area. **A** – Updated geological map of the study area (based on Biely et al., 1992; modified according to Tulis & Novotný, 1998, Appendix 1; Olšavský, 2008, Fig. 41, 79, 80, 81; and our mapping) overlain on the hillshade model from LiDAR data (source: ÚGKK SR), with marked-out sampling sites with concentrations of Pb, Zn, and Cu above 100 ppm based on chemical analysis (Kantor, 1957; Hanáček, 1963; Ivanov et al., 1965) and sites of photos from photos in Fig. 4, the black rectangle denotes the extent of figure C. **B** – Same geological map from Fig. 1A with added sampling sites for spectral analysis of Pb, Zn, and Cu concentrations above 1 ppm. **C** – Close-up view of the geological map in the vicinity of the Blue Cave. **Legend:** Faults: **1** – thrusts; **2** – other fault types, **a** – known, **b** – assumed, **c** – covered; Quaternary: **3** – alluvial plain deposits; **4** – slope deposits; **5** – lower fluvial terraces; **6** – middle fluvial terraces; **7** – upper fluvial terraces; Middle Triassic: **8** – Reifling Fm., basinal limestones with chert nodules; **9** – Ramsau Fm., dolomites; **10** – Gutenstein Fm., limestones and dolomites; **11** – 'Čierny Váh carbonates', dolomites with occasional limestones; Lower Triassic: **12** – Šuňava Fm., variegated sandstones, mudstones, shales, and limestones; **13** – Benkovo Fm., sandstones and shales; **14** – Malužiná Fm., variegated sandstones and shales; **15** – Malužiná Fm., volcanics of basaltic to andesitic composition. See appendices for the original geochemical data.

borehole Ma-2, Biely (1964) reported the presence of Middle Triassic carbonates and the underlying Permian volcanics separated by a thrust (Fig. 3).

The tectonic complexity of the Hronic Unit near the Blue Cave has given rise to a broad range of interpretations of the internal architecture of the unit. These include (1) two tectonic units separated by a broad deformed zone containing tectonic slices (e.g. Biela, 1960, p. 24–27; Biely, 1960, 1962); (2) three tectonic units (e.g. Biely, 1963, 1964, p. 28–29); (3) two subordinate units belonging to the lower tectonic unit, overridden by the upper tectonic element (e.g. Biely, 1976, p. 60–64); (4) or two tectonic units with the lower one arranged into an array of tectonic slices (e.g. Badár et al., 1965, p. 69–72; Vozár et al., 1983, p. 83–85; Tulis & Novotný, 1998, p. 70–71, Appendix 1). Currently, three subordinate Hronic nappes are recognised (Fig. 1C), but doubts about their validity are still present (Biely et al., 1992, 1997, p. 147–149; Havrila, 2011, p. 13, Fig. 1). Recent findings of additional internal tectonic complications cast further doubt on this interpretation, as these would necessitate recognition of four or more subordinate nappes (Olšavský, 2007a, 2007b, 2008, p. 168–173).

The complexity of the Hronic Unit in the area also led to conflicting depictions of the geology near the Blue Cave in two of the most recent geological maps (Biely et al., 1992; Appendix 1 in Tulis & Novotný, 1998). According to the map of Biely et al. (1992), the carbonate block that hosts the cave is bounded by steep N-S-striking faults. In contrast, the same carbonates are bounded by E-W-striking thrusts in the map of Tulis and Novotný (1998, Appendix 1). The structural data from the cave and its vicinity could assist in resolving the difficulties in the interpretation of the internal structure of the Hronic Unit.

The precise arrangement of fluvial terraces near the Blue Cave is unclear. The known maps showing the Quaternary terraces (Čechovič, 1942; Ilavský & Ilavská, 1949; Jeremenko, 1956; Kubáň, 1956; Hanáček, 1963; Vozár, 1970, 1974; Biely, 1976; Kantor & Ďurkovičová, 1977; Vozár et al., 1983; Biely et al., 1992) tend to display a different number of terrace levels and even a different spatial distribution of terraces. Therefore, further work was required to verify the extent of terrace deposits.

## Methods

To resolve the uncertainties in the geological setting of the Blue Cave obvious from the different geological maps, additional geological mapping was employed. In the broader area, the main tool used for the remapping was the LiDAR-based Digital Elevation Model (DEM, source: ÚGKK SR). LiDAR-based mapping aimed to determine the extent and distribution of the Quaternary sediments, with a particular focus on the stream terraces. Field mapping was employed in a radius of approximately 500 m from the cave and additionally around the Boca Stream, approximately 1 km downstream from the cave. Field mapping was used to further verify the extent of the terraces and to ascertain the structural position of the Čierny Váh carbonates within the Hronic Unit. The surface observations were further supplemented by the maps from unpublished reports and subsurface data.

The unpublished works (Kantor, 1957; Hanáček, 1963; Biely, 1964; Ivanov et al., 1965) are written in Slovak and Czech, so we digitised the data most pertinent for this paper to improve their availability for the wider scientific community. The digitised data were used in the figures and interpretations, and are provided as appendices to this paper. The maps showing the sites of the collected samples were georeferenced, and the results of chemical and semiquantitative spectral analyses were attributed to each site as a set of attributes in the QGIS software version 3.34.11 (QGIS Development Team, 2024). The detected amounts of Pb, Zn, and Cu in the chemical analysis were displayed on the map as individual symbols, while stacked bar charts were used to display detected amounts of Pb, Zn, and Cu in semiquantitative spectral analysis (Figs. 2A–C). The locations of boreholes Ma-1 and Ma-2 were also marked on the map (Figs. 1C and 2A–C), and the borehole logs were re-drawn as best as possible, since some parts of them have faded out. The results of chemical and semiquantitative spectral analyses from the borehole cores were added to the appropriate depth intervals of the borehole logs (Fig. 3).

We studied the Čierny Váh carbonates directly in the cave, where six samples (MM-1 to MM-6) were collected for the study in thin sections, and of those, four samples were also processed for the whole-rock analysis of major rock components (Tab. 1). One surface sample (MM-7) from the brecciated layer above the cave entrance No. 1 was also collected for thin-section study and whole-rock analysis. Thin sections and whole-rock analyses were prepared in the Geoanalytic Laboratory of the State Geological Institute of Dionýz Štúr in Spišská Nová Ves. The thin sections were studied using an optical microscope for the microfacial characterisation. In the whole-rock analysis, loss on ignition was determined by using gravimetric analysis and chemistry of the major components was determined by x-ray fluorescence spectrometry.

The 3D model of the cave and the surface around the entrances was scanned by the SLAM-based scanner GeoSLAM Zeb Horizon. The scanner has a reach of 100 meters, a speed of 300,000 points per second. The resultant point cloud was composed of the five parts for the cave and a single part for the surface. Each cave section was referenced to at least four fixed survey stations of the centerline. The centerline in quality UISv2 6-0-BCEF and mean error on a loop of 0.49 % was obtained by a compass method utilising calibrated DistoX2 and PocketTopo software (Heeb, 2020), then processed in Therion software (Mudrák & Budaj, 2010). The cave entrances were surveyed by the GNSS method with RTK correction using Trimble Geo 7x H-Star.

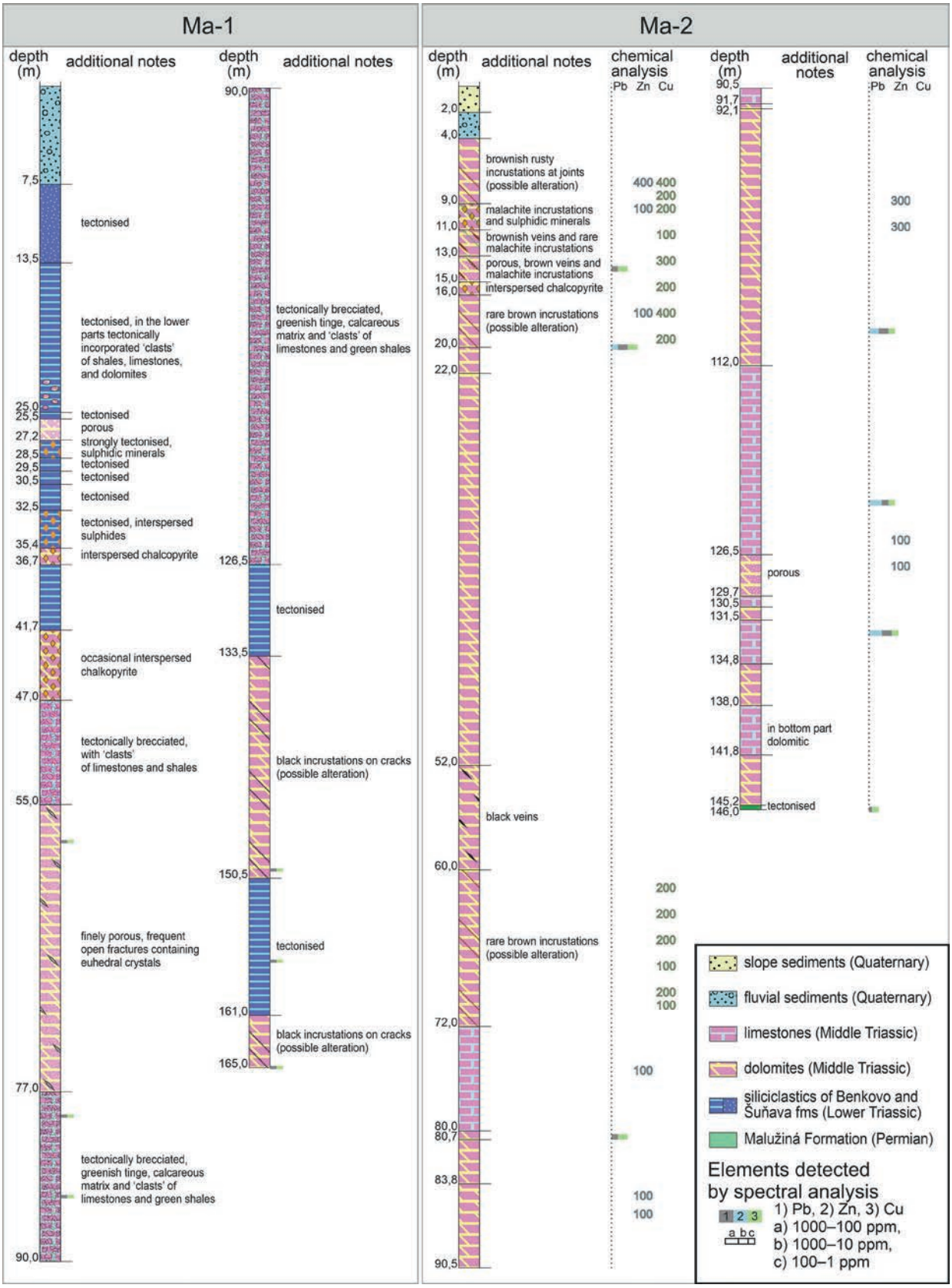


**Fig. 3.** Interpreted borehole logs from Biely (1964) with additional geochemical data from Ivanov et al. (1965). See the appendices for the original logs.

**Tab. 1**

Chemical composition of the samples from the host rock of the Blue Cave (LOI – loss on ignition).

| [%] | MM-1 | MM-3 | MM-4 | MM-6 | MM-7 |
|---|---|---|---|---|---|
| $SiO_2$ | 0.16 | 0.76 | 0.41 | 0.85 | 2.54 |
| $Al_2O_3$ | 0.06 | 0.39 | 0.16 | 0.42 | 0.79 |
| $Fe_2O_3$ | 0.52 | 0.23 | 0.14 | 0.15 | 0.58 |
| CaO | 29.8 | 30.5 | 30.4 | 29.8 | 32.3 |
| MgO | 21.6 | 20.6 | 21.3 | 21.5 | 18 |
| $TiO_2$ | < 0.01 | 0.02 | < 0.01 | 0.02 | 0.06 |
| MnO | 0.10 | 0.02 | 0.04 | 0.02 | 0.06 |
| $K_2O$ | < 0.05 | 0.12 | 0.06 | 0.15 | 0.25 |
| $Na_2O$ | < 0.2 | < 0.2 | < 0.2 | < 0.2 | < 0.2 |
| $P_2O_5$ | 0.02 | 0.01 | 0.01 | 0.02 | 0.02 |
| LOI | 47.6 | 47.3 | 47.3 | 46.9 | 45.3 |

Two approaches were used to measure structural discontinuities in the Blue Cave: measurements from the 3D model of the cave and field measurements directly in the cave. The measurements from the 3D model were done using the Compass plugin (Thiele et al., 2017) in CloudCompare ver. 2.13.1 (2023). Structural measurements of identified bedding planes, joints, fractures, faults, and slickensides in the cave were taken with an accuracy of ± 2° by the Freiberg Geological Structural Compass. The data were then processed in the software Stereo32 ver. 1.0.1 (Röller & Trepmann, 2003).

The inventory of solution cave morphologies and their spatial distribution, their relation to structural discontinuities, and the adjacent surface landforms, were used to reconstruct the processes of the origin and development of the cave. Also, lithological facies of preserved fluvial sediments contribute to clarifying the former hydrographical conditions during the cave formation. Using the cave map of P. Imrich, J. Szunyog, and others from 2016 (published in Šmoll, 2017), we studied the cave pattern. We determined the cave pattern and connectivity of cave passages based on the graph analysis applied to cave topology by Howard (1971). The period of formation of the cave was estimated based on a comparison of its relative height above the recent Boca Stream's streambed with the relative height and estimated age of stream terraces and cave levels in the nearby areas.

## Results

### *Geological mapping*

The geological mapping revealed that the Čierny Váh carbonates of the Blue Cave are not in a normal stratigraphic position, but are instead tectonically sandwiched between older non-karstic rocks. The Middle Triassic carbonates crop out as an isolated block on the left bank of the Boca Stream, flanked by the Upper Permian volcanics in the southwest and the Lower Triassic siliciclastics in the northeast. The tectonic position of the Čierny Váh carbonates between older rocks – subjacent volcanics and superjacent siliciclastics, can be deduced from their map expression (Figs. 2A and C). Additionally, the Upper Permian volcanics and the overlying Middle Triassic carbonates are in direct contact, without the stratigraphically intervening the Upper Permian to the Lower Triassic siliciclastics. The siliciclastics are also absent in the borehole Ma-2 (Biely, 1964), which penetrated through the Čierny Váh carbonates directly into the tectonic contact with underlying volcanics (Fig. 3). The absence of siliciclastics is particularly striking considering that the borehole is situated less than 15 m from the mapped contact of the siliciclastics and the Čierny Váh carbonates. Moreover, a small exposure of intensively deformed rocks was found at the contact between the Čierny Váh carbonates and siliciclastics, circa 100 m NE from the cave (Figs. 2C and 4A). Hence, we interpret the Middle Triassic Čierny Váh carbonates of the Blue Cave as a thrust sliver wedged between older rocks the underlying Permian volcanics and overlying Lower Triassic siliciclastics (Figs. 2A and C). Additional evidence of substantial thrusting can be found further from the cave and near the mines in the Olovienka Ravine.

Several tectonic slices of volcanic and siliciclastic rocks enclosed within dolomites were mapped near the Olovienka Ravine. On the left bank of the Boca Stream, approximately 150 m upstream from the ravine, Hanáček (1963) mapped siliciclastics within the dolomites, which do not appear in the subsequent geological maps. During our mapping, we found a de-vegetated slope that exposed not only the fragments of siliciclastics but also abundant fragments of volcanics (Figs. 2A and 4B). A small fan at the foot of a gully formed within carbonates also contained numerous clasts of volcanics, indicative of their upslope exposure. Abundant rauhwacken (cellular dolomites) occurring within the carbonates provide further evidence for the tectonic reworking of the rocks (Fig. 4D). Thanks to the subsurface data, the thrust fault mapped on the opposite bank can be traced to the mines in the Olovienka Ravine (Fig. 2A). On the left bank, the thrust is mappable due to the presence of the deformed siliciclastic rocks (Figs. 2A and 4C) older than the surrounding Čierny Váh carbonates. On the right bank, the siliciclastics were not

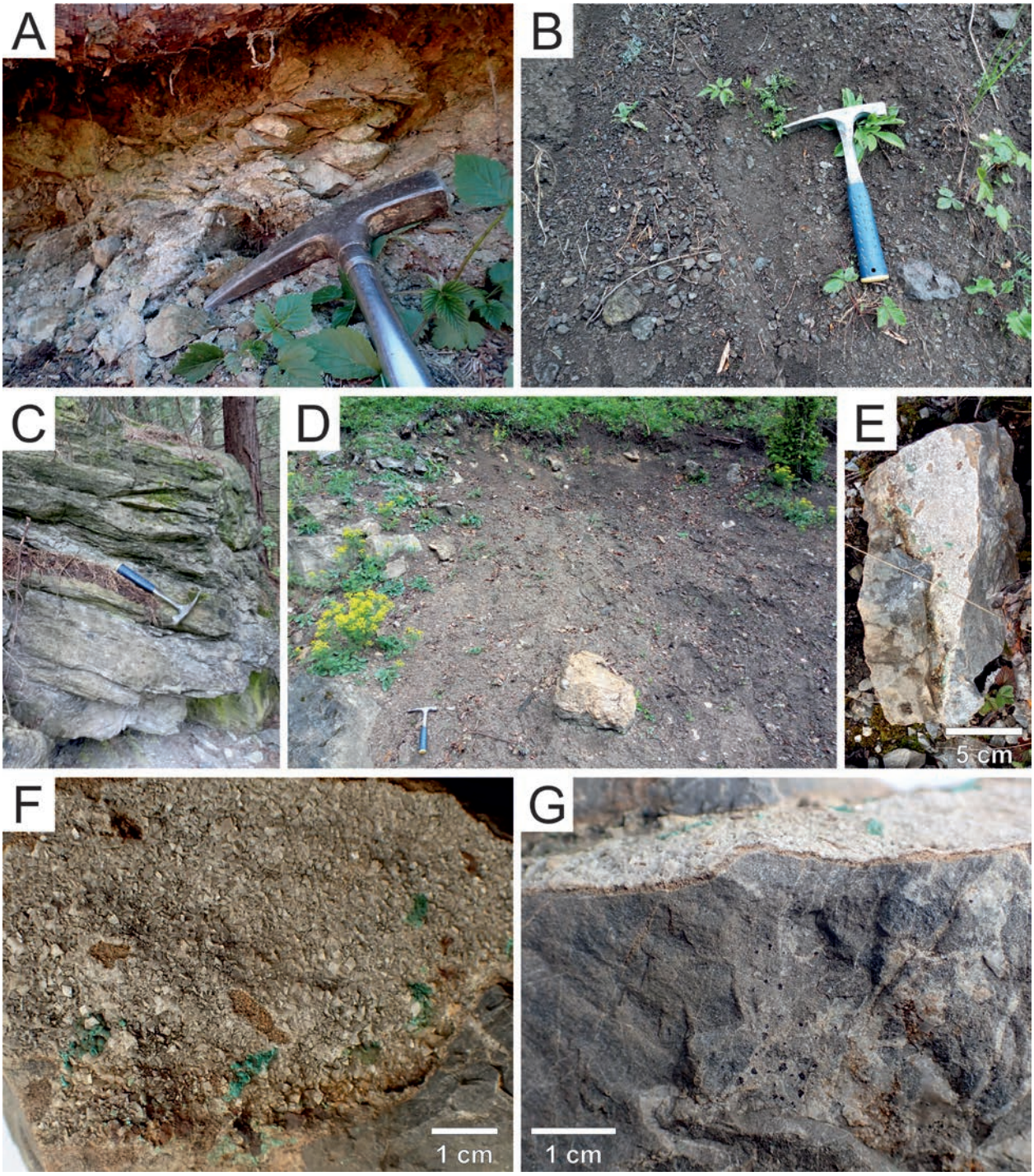


**Fig. 4.** Geological observations from the surface of the study area. **A** – Small exposure of tectonised rock at the contact between the underlying Middle Triassic carbonates and overlying Lower Triassic siliciclastics. **B** – Fragments of the Permian volcanic rocks exposed at the foot of a devegetated slope that occur between the Middle Triassic carbonates. **C** – Strongly tectonically stretched Lower Triassic siliciclastics that from a tectonic slice between the Middle Triassic carbonates. **D** – A zone containing yellowish fragments of tectonised carbonates (rauhwacken) within the grey, relatively undeformed carbonates exposed at the foot of a devegetated slope. **E** – Photograph of the malachite-bearing dolomite found in the talus below the outcrop near the Blue Cave. **F** – Close-up view of the vein in the dolomite containing malachite, euhedral calcite crystals, and rusty brown iron oxides. **G** – Close-up side view of the vein from figure F, macroscopic iron oxide crystals can also be seen in the rock below the vein. All photos by J. Littva.

mapped, but the borehole Ma-1 (Biely, 1964) penetrated several siliciclastic rock packages within the carbonates (Fig. 3). The siliciclastics were also observed in the walls of one of the mines in the Olovienka Ravine (Kantor, 1957), enabling us to interpolate the continuation of the thrust to this location. We interpret these observations as evidence of thrusting that disrupts the Čierny Váh carbonates and involves slices of older siliciclastics and volcanics.

Our mapping and the subsurface data from the unpublished reports have revealed a substantial tectonic reworking of the Čierny Váh carbonates. These rocks show distinctive internal deformation, with the Čierny Váh carbonates both incorporating and being incorporated into packages of the older siliciclastics and volcanics. Notably, these reworked rocks are positioned between the thick packages of less deformed rocks – the underlying Upper Permian volcanics and the Triassic carbonate suite of the overriding nappe (Figs. 1C and 2A).

Based on the observations from the DEM and field mapping, we mapped several terrace surfaces near the Blue Cave (Figs. 2A and C). The highest number of terrace risers seems to be preserved closer to the Blue Cave, at the confluence of the Boca Stream with its right tributary, the Malužiná Stream. Further from this point, the terrace preservation seems to be poorer (Figs. 2A and C). Unfortunately, this site is marked by extensive formation and collapse of karst features, which caused irregularities in the previously flat terrace surfaces, hampering the terrace mapping. Moreover, the area underwent considerable anthropogenic landscape modifications – the construction of roads, housing, and a recreational area. Resulting cut-and-fill earthworks resemble the terrace risers and benches, and thus complicate the determination of terrace levels. Therefore, instead of distinguishing individual terrace levels, we grouped the terraces into three categories: lower terraces, middle terraces, and upper terraces. Their relative heights above the recent streambed are 2–10 m, 10–20 m, and 20–30 m, respectively. Poor exposure of terrace risers prevented us from estimating the thickness of fluvial gravels on the terrace levels. A minimal gravel thickness of at least 2 meters can be assumed for one of the middle terraces, based on the presence of a two-meter-thick interval of fluvial gravels in borehole Ma-2 (Biely, 1964). The gravel thickness and the bedrock exposures in the terrace risers suggest that most of the terraces are strath-type terraces, possibly excepting some of the lower terraces.

Further from the cave, the terraces were mapped based on the DEM observations combined with data from previous geological maps (Jeremenko, 1956; Kubáň, 1956; Hanáček, 1963; Biely, 1976, p. 19; Vozár et al., 1983). Further verification was necessary for a flat surface at the left bank that extends from approximately 750 m downstream of the Blue Cave to approximately 200 m downstream of the Olovienka Ravine. The surface was mapped as a terrace only in the map of Hanáček (1963), but granitic pebbles were found in the geotechnical boreholes made at the same surface (Lošonská, 1984), corroborating the map. We mapped fluvial gravels at the flat surface, confirming Hanáček's (1963) map. Based on its relative height above the recent streambed (20–30 m), the terrace was assigned to the upper terraces.

The known parts of the Blue Cave are most closely associated with the upper and middle terraces. The elevation span of the documented cave spaces (between 742–767 m a.s.l.) predominantly corresponds to the position below the upper terraces, roughly at the level of the middle terraces. Some of the low-lying parts of the cave reach the level of the lower terraces as well. The association of the cave with the upper and middle terraces can also be observed in the map view (Figs. 2A and C).

### *Mineralogy and geochemistry of the area*

In the studied area, the occurrences of the sulphide or malachite and azurite were noted at three localities: mines in the Olovienka Ravine, Malužinská Cave, and the Blue Cave. Sulphide minerals (galenite, sphalerite, pyrite, marcasite) were reported near mines (Kantor, 1957; Hanáček, 1963; Kantor, 1975) and in the nearby borehole Ma-1 (Figs. 2A, B, and 3). Cu sulphides (chalcopyrite and tetrahedrite), and also malachite and azurite occur in carbonates drilled by borehole Ma-2 at depths of 9–10 m and 15–16 m (Fig. 3). The dolomites covered by thin incrustations of malachite and azurite were observed in two surface outcrops (Hanáček, 1963; Ivanov et al., 1965), both associated with caves. The first one is located near the entrance of the Malužinská Cave (Figs. 2A and B), which presently lacks known spaces with coloured speleothems (Bella et al., 2014). The second outcrop, located less than a hundred meters from the Blue Cave, is presently completely covered by vegetation, preventing direct observation of the malachite or azurite. In a talus below the outcrop, we found a dolomite containing malachite (Figs. 4F and G) as well as small unidentified black minerals (Fig. 4G). Both mineral types are occasionally disseminated in the dolomitic rock mass. However, they are typically associated with veins in the dolomitic rock, along with the rusty-brown residue, possibly a weathering product of the sulphide minerals (Figs. 4F and G).

Following the distribution of minerals, the elevated trace quantities of Pb, Zn, and Cu also cluster approximately around mines in the Olovienka Ravine, the Malužinská Cave, and the Blue Cave (Figs. 2A–C). Hanáček (1963) and Ivanov et al. (1965) detected elevated amounts of copper utilising chemical analysis (up to 500 ppm) and semiquantitative spectral analysis (up to 1000 ppm) from both the outcrop and borehole samples. The trace amounts

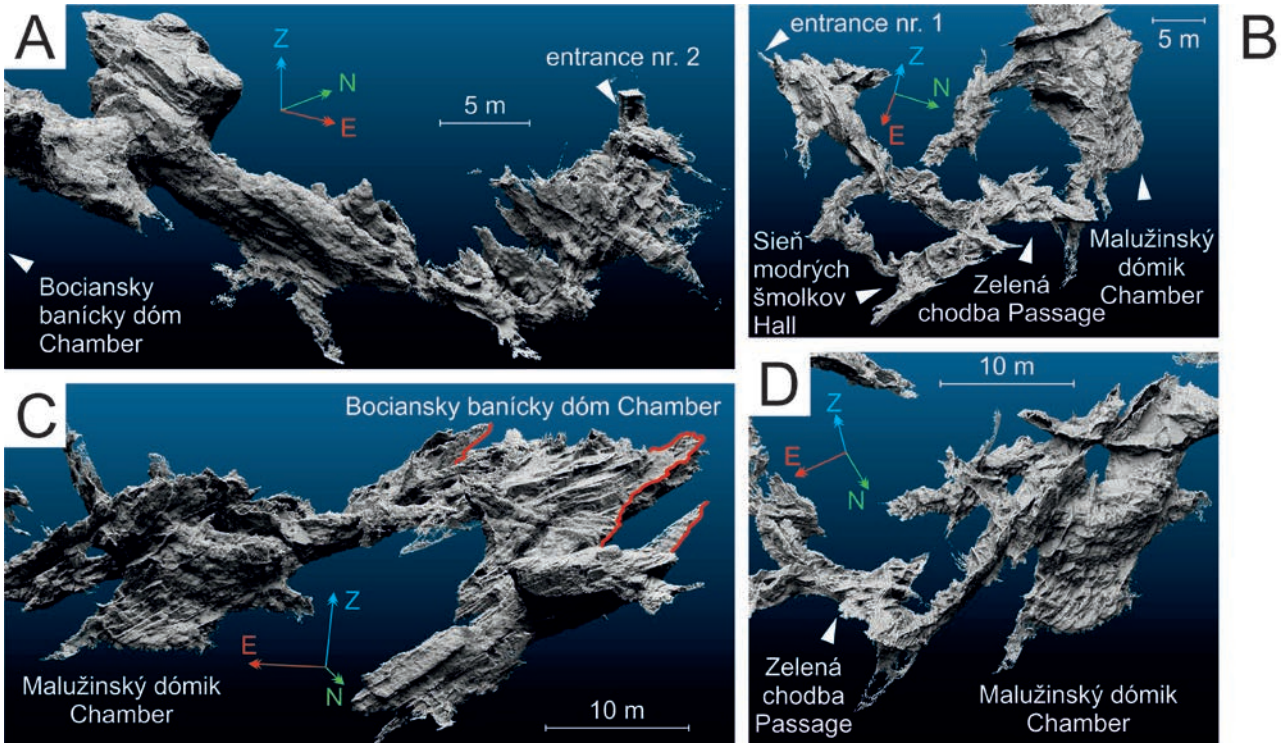


**Fig. 5.** Parts of the 3D model of the Blue Cave processed and viewed in CloudCompare (2023). **A** – The northwestern part of the Blue Cave formed in the bedded dolomites. Left side: Parts of the cave around the entrance nr. 2 controlled by the combination of joints and bedding. Right side: The bedding-controlled inclined passage leading to the Bociansky banícky dóm Chamber. **B** – The southeastern part of the Blue Cave, formed mostly in massive dolomites, with branching and intersecting passages that follow the bedrock fractures. **C** – A view of the Bociansky banícky dóm Chamber with thrust-and-fold structure (thrust outlined in red colour) and northwestern wall of the Malužinský dómik Chamber, exposing bedded dolomites. **D** – A view of the NE-SW fault that crosses the Malužinský dómik Chamber and separates the bedded and massive dolomites.

of lead are the highest near the mines. The same is true for trace amounts of zinc, although lower trace amounts of zinc were detected around the Malužinská Cave (Figs. 2A and B) and in the borehole Ma-2 (Fig. 3). Copper was detected around all three sites in trace amounts, but the rocks around the Blue Cave and in the borehole Ma-2 contain the highest concentration of copper. In the borehole, up to 400 ppm Cu and Zn, as well as < 100 ppm of Pb, were detected in dolomites at the depth interval of 6 to 20 m (Fig. 3), i.e. 746 to 734 m a.s.l. Thus, the Blue Cave is closely associated with the mineralised zone in the nearby borehole Ma-2, which contains Cu-sulphides, malachite, and trace amounts of Zn, Cu, and Pb.

### *Geological observations from the cave*

The cave is hosted in grey and dark grey, sporadically brecciated dolomites, typically penetrated by a network of thin white calcite veins. The dolomites can be separated into two types based on the presence or absence of bedding. While the dolomites in the northwestern part of the cave are markedly bedded, in the southeastern part, the dolomites are massive-bedded (Figs. 5A–D and 7A). Both dolomite types markedly influence the character and morphology of the passages developed within them, as we will discuss later. The bed thickness in bedded dolomites generally ranges between 5–20 cm, with some thinner beds (2–3 cm) in between. Generally, the beds dip 25–45 degrees to the east, with some variations to the NE near the entrance and to the SE in the Malužinský dómik Chamber (Fig. 6). The dip and strike of the massive-bedded dolomites could not be observed. Both dolomite types are chemically similar, containing more than 20 % MgO (Tab. 1), and both are also microscopically similar. They comprise dolomicrosparite (samples MM-2, 3, and 6; Figs. 8A and C), breccia (samples MM-4 and MM-7; Fig. 8B), and dolosparite (samples MM-1 and 5; Fig. 8D), with sparry veins, dark brown stains after iron oxides, and microstylolites. The sample MM-5 was not completely recrystallised into dolosparite and contained patches of unrecrystallised dolosparite as well as fine pores (Fig. 8D). In the samples MM-3 and MM-6 from the bedded dolomites, dolomicrosparite has an occasional markedly directional texture, representing the bedding micrite (Fig. 8C). No fossils were found in the rocks and thin section, but based on the stratigraphic position above the Lower

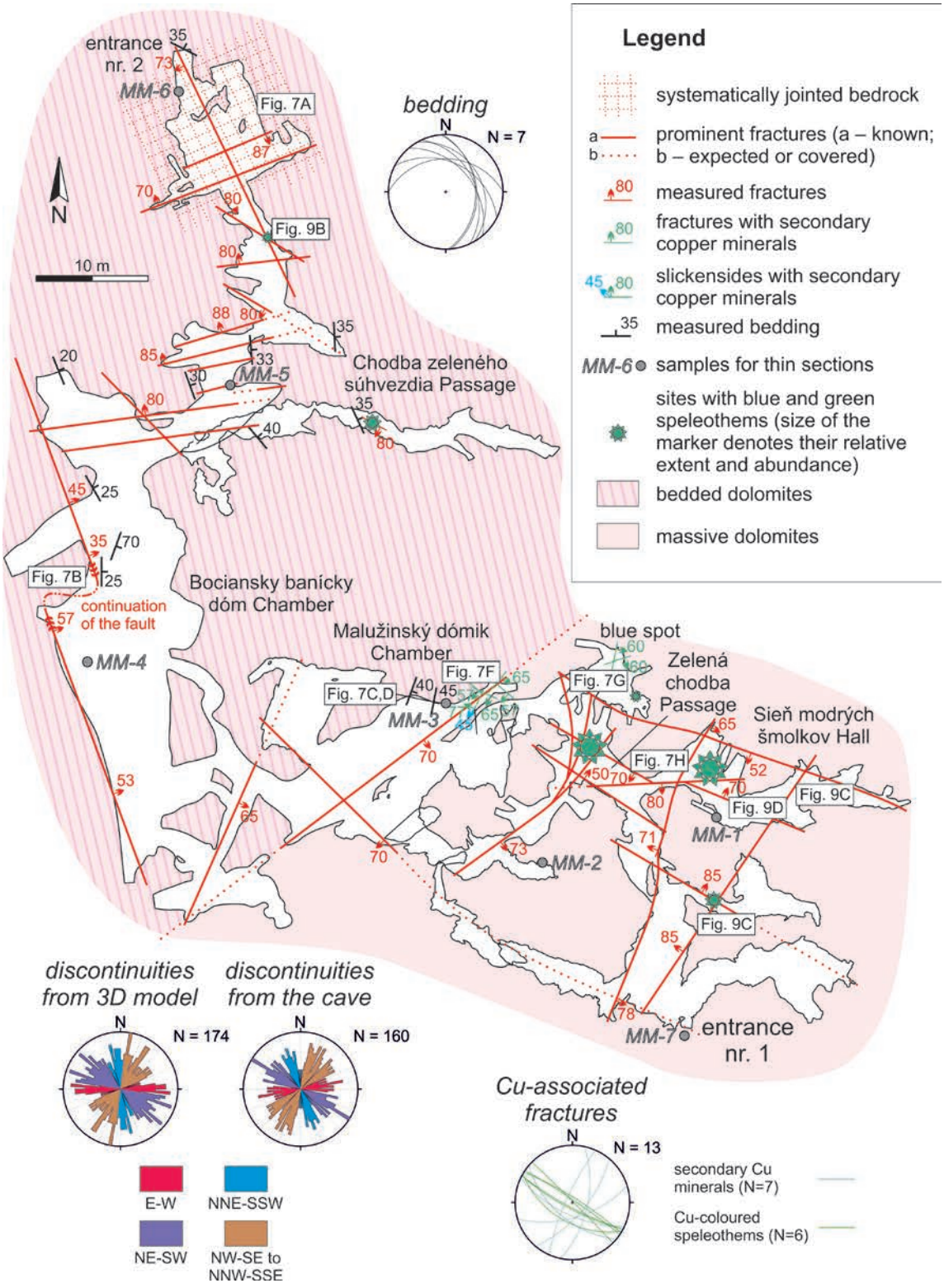


**Fig. 6.** Cave plan of the Blue Cave with marked-out geological features denoted in the legend and placement sites of photos from Figs. 7 and 9. The figure also includes two lower-hemisphere equal-angle stereographic projections and two rose diagrams with equal area-scaling generated in the Stereo32 software (Röller & Trepmann, 2003). The stereographic projections show great circles of fractures associated with the malachite and fractures associated with blue and green speleothems, and the bedding attitudes. The rose diagrams show strikes of the fractures measured from the 3D model and from the cave. The fracture sets are grouped into four colour-coded categories that are further discussed in the text.

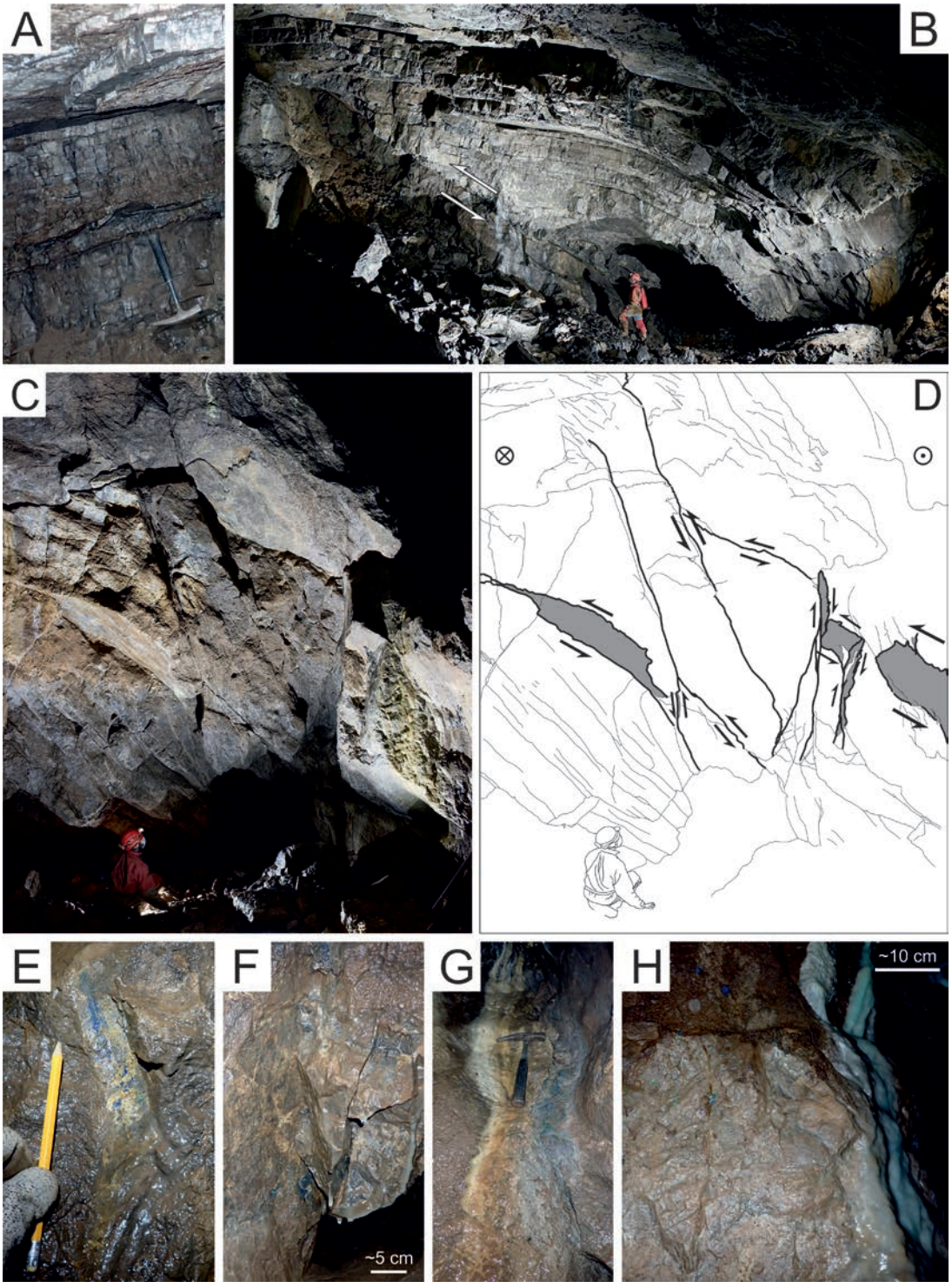


**Fig 7.** Lithological, structural, and mineralogical features observed in the Blue Cave. **A** – Bedded dolomites observed near the entrance nr. 2. **B** – Fold-and-thrust structure in the Bociansky banícky dóm Chamber, white half arrows denote movement sense. **C** – Rock wall in the Malužinský dómik Chamber exposing side view of the NE-SW-striking fault that dismembers a low-angle thrust fault. **D** – Interpreted sketch of figure C, with the dip slip component of movement denoted by half arrows and the strike slip component denoted by the circles (circled cross and circled dot – away from the viewer and towards the viewer, respectively). **E** – Slickenside of the fault shown in figures C and D, with calcite and possibly also azurite accretion steps indicating dextral movement sense. **F** – Azurite-bearing fractures in a crawlway concealed in the shadow in figure C. **G** – Fractured bedrock mineralised by the malachite and azurite near the 'blue spot'. **H** – Malachite and azurite occurring near the greenish speleothem in the Zelená chodba Passage. Photos: A, E, F, and H by J. Littva; B and C by P. Staník; G by L. Dušeková.

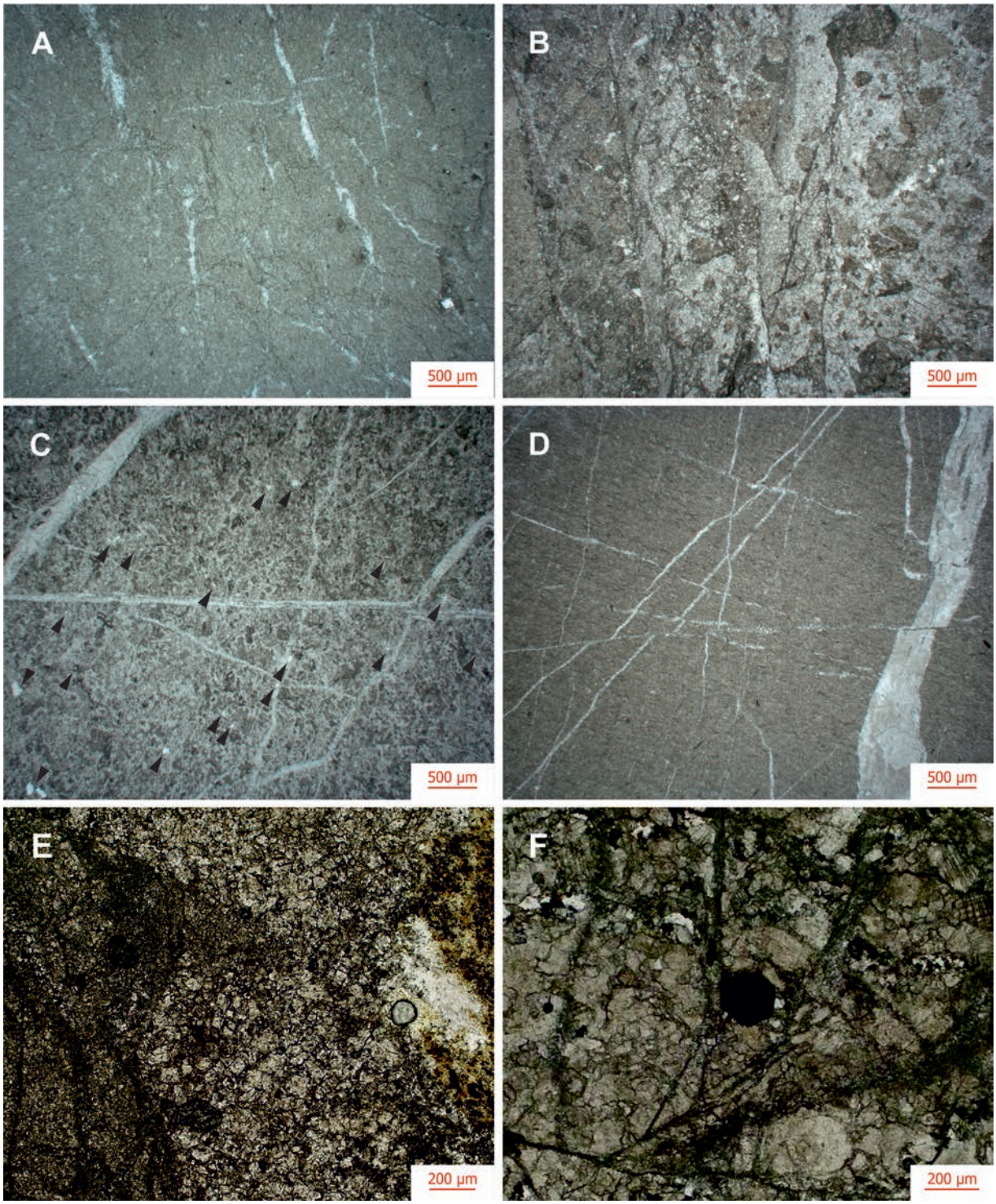


**Fig. 8.** Microphotographs of samples taken from the host rock of the Blue Cave, plane polarised light. **A** – Dolomicrosparite in the sample MM-3. **B** – Tectonically brecciated dolomicrite in the sample MM-4. **C** – Finely porous dolosparite with patches of unrecrystallised dolomicrite in the sample MM-5, pores marked by the black arrows. **D** – Bedding micrite in the sample MM-6. **E** – Euhedral dolomite crystals forming sparry matrix and iron oxides filling the intercrystalline pores, between the larger, less dolomitised clasts on the left and the right side of the picture. **F** – An euhedral iron oxide crystal that grew within the dolosparite of the sample MM-1. Photos: A–D by Ľ. Gaál; E and F by J. Littva.

Triassic rocks, we infer the Anisian age for the carbonates that host the Blue Cave.

In the thin section of the sample MM-7, we observed mineralisation that could be linked to the blue and green speleothems. Although the samples MM-4 and MM-7 are both breccias, they are markedly different. In the former, the dolomite clasts are compositionally uniform and have a brownish colour, and the crystals in the matrix are anhedral to subhedral and chiefly translucent (Fig. 8B). Based on the proximity to the thrust described below, the breccia in the sample MM-4 is likely tectonic. In the sample MM-7, the MgO concentration is slightly lower than in the sample MM-4, while concentrations of CaO and $SiO_2$ are slightly higher (Tab. 1). As the sample contains sparser, compositionally varied clasts, including the clasts of undolomitised limestone, it is likely of sedimentary origin. The matrix in the sample MM-7 is predominantly composed of euhedral crystals (Fig. 8E). The iron oxides filling the intercrystalline spaces among the matrix crystals lend the sample an overall rusty brown colour. Hence, the iron-oxides are not merely the primary constituent of the rock, but a result of secondary mineralisation, which exploited the intercrystalline porosity of the matrix.

In the sample MM-1, taken from the part of the cave most extensively decorated by blue and green speleothems, the mineralisation is even more intense. Instead of exploiting the porosity, up to 200 μm big (Fig. 8F) euhedral grains of the iron oxides developed directly among the grains. Despite the evidence of the mineralisation in the Čierny Váh carbonates, malachite and azurite were not directly observed in any of the thin sections from the collected samples.

In the cave, we encountered two major tectonic structures that have broader implications for the geology of the wider area. A conspicuous N-S-striking fold-and-thrust structure is observable both in the 3D scan and also directly in the Bociansky banícky dóm Chamber (Figs. 5C and 7B). It separates massive dolomites in the footwall from the brecciated dolomites in the hangingwall. In contrast to the thrusts observed on the surface, no older siliciclastic or volcanic rocks were incorporated into this structure. The second major structure is a steep NW-SE strike-slip fault zone guiding the Malužinský dómik Chamber. It separates the bedded dolomites prevalent to the northeast of the fault from the massive dolomites in the southeast (Fig. 5D). The faults of this zone dismember the thrust faults associated with the fold-and-thrust structure described above (Figs. 7C and D), constraining the post-thrusting age of the strike-slip fault. Although these two conspicuous structures predispose two of the three main chambers and halls of the Blue Cave, elsewhere, the cave spaces are guided by other tectonic structures.

The fractures that control the orientation of the cave spaces are oriented in four principal directions: NE-SW, NNW-SSE to NW-SE, NNE-SSW, and E-W (Fig. 6). In the passage leading from the entrance nr. 2 to the Bociansky banícky dóm Chamber, the E-W-striking sub-vertical (> 80°) fractures were the most frequently measured. The E-W fractures frequently predispose appearance of some salients of the main passage and also coincide with the passage's abrupt narrowings and widenings (Fig. 6). However, the main passage tends to follow the NW-SE to NNW-SSE fractures, which are most pronounced near the entrance nr. 2 in the form of the systematic joints (Fig. 6). Some of the blind branches and salients of both the main passage and Chodba zeleného súhvezdia Passage are also predisposed to this type of discontinuities (Fig. 6). From the Malužinský dómik Chamber to the entrance nr. 1, the fracture pattern changes, resulting in the different passage pattern of the cave. Although all fracture types were noted here, two fracture types are the most prominent: (1) steeply-dipping to subvertical (60°–90°) NE-SW fractures and (2) moderately to steeply-dipping (40°–80°) NW-SE to NNW-SSE fractures (Fig. 6). These fracture types guide most of the network of passages and their salients between the entrance nr. 1 and Malužinský dómik Chamber (Figs. 5A–D and 6).

While the fold-and-thrust structure is unmineralised, the malachite and azurite appear on the NW-SE and NE-SW discontinuities, and blue and green speleothems are associated with the NW-SE fractures. Malachite, azurite, and occasionally black minerals (likely iron oxides) are extensively associated with the NE-SW fault (Figs. 6 and 7E–H). The azurite appears to form an accretion step behind the calcite steps on the slickenside associated with the NE-SW fault (Fig. 7E), indicative of a dextral strike-slip. Other similarly oriented slickensides from other parts of the cave also bear dextral kinematic indicators, but lack the azurite or malachite. On the other hand, the malachite and azurite are also associated with some NW-SE-oriented fractures (Fig. 6). In contrast, the blue and green speleothems are hosted exclusively by the NW-SE fractures (Fig. 6). The speleothems appear most extensively in Sieň modrých šmolkov Hall and Zelená chodba Passage (Figs. 6, 9A and D). Some smaller blue and green speleothems were also observed in the Chodba zeleného súhvezdia Passage and near the entrances nr. 1 and 2 (Figs. 6, 9B and C).

### *Cave morphology and clastic sediments*

The Blue Cave is an inactive phreatic cave with several loops (*sensu* Ford, 1977, 1988, 2000; Ford & Ewers, 1978), in places with steep parallel fractures enlarged into halls and chambers that were later remodelled by collapse. In the direction of the former water flow, the upward leading parts of the loops are mostly controlled by fractures, while the

downward leading parts are controlled by bedding planes of host rock carbonates. Downward inclined oval passages were enlarged from initial bedding-plane anastomoses. Small lateral conduits, featured by a channel-like ceiling and floor covered by fine-grained sediments, sloping along inclined bedding planes, correspond to a morphology and structural control of bedding-plane anastomoses (*sensu* Bretz, 1942; Ewers, 1966; Palmer, 2007 and others). Some of these were formed later than the main cave passages, probably by injected floodwater. Large scallops on the rock wall in the northern part of the cave indicate a former water flow that moved downwards into the bedding-plane conduits. Ceiling solution pockets are developed mostly in the lower part of the loops, mainly in places where they are cut by transverse fractures (Fig. 10D). Conversely, larger ceiling pockets to cupola-like cavities are mostly observed in the upper part of the loops.

The ground plan of the cave shows three partially different parts: (1) a network-like pattern in its south-eastern part composed of main passages controlled mostly by parallel and intersecting fractures developed in massive dolomites; (2) a fold-and-thrust-controlled spacious, elongated chamber-like cavity in its western part (Bociansky banícky dóm Chamber); (3) crossing and less interconnected passages in its northern part controlled mostly by fractures, in some places influenced by bedding planes. Many small lateral passages are represented by dead-end fissures or bedding-plane anastomoses, considered as floodwater injection features (*cf.* Palmer, 1991, 2007).

A degree of connectivity of the whole cave pattern is given by the quantitative parameters  = 0.081,  = 1.096, and  = 0.374 calculated based on the graph analysis applied to the cave pattern according to Howard (1971). A slightly higher degree of connectivity of the labyrinth-like part is given by parameter values  = 0.097,  = 1.163, and  = 0.404. For a large cave network with a very high degree of interconnection and few dead-end passages or exits, these parameters reach the values 0.25, 1.5, and 0.5. For caves with few loops and a dendritic channel pattern, they reach the values 0.1 and 0.33 (Howard, 1971).

The largest cavity in the south-eastern network-like part of the cave is the Malužinský dómik Chamber, which is mainly predisposed by the NW-SE fault and genetically related fractures. A spacious, elongated cavity called the Bociansky banícky dóm Chamber in the western part of the cave is the cave's most voluminous.

Inwardly sloping smooth solution facets (Fig. 10B) – planes of repose *sensu* Lange (1963) developed on both sides of the passage between the Bociansky banícky dóm and Malužinský dómik chambers. They were formed during the sedimentation of fine-grained insoluble rock particles on the floor and inwardly sloping parts of the cave walls. These particles protect the covered bedrock from further dissolution.

Inclined wall half-tube notches, limited in extent, are visible in parts of the cave formed in bedded dolomites and controlled by bedding planes (Fig. 10C, preserved on the right side of the passage). They can probably be classified as paragenetic solution ramps, which form in a phreatic environment at the surface of the sedimentary floor when the dissolution of the wall between a sedimentary fill and the ceiling is preferential (*cf.* Farrant & Smart, 2011). Smaller wall water-table notches originated in standing water (*cf.* Ford, 1988; Lauritzen & Lundberg, 2000 and others) and occur only around small wall niches.

The stalactites in the Sieň modrých šmolkov Hall bear marks of the former flooding of the cave that postdates their growth. The stalagmites are covered by a thin veneer of fine-grained sediments, indicating the level of the floods (Fig. 9D).

The floor of the lower part of the loops is mainly covered by fine-grained sediments deposited from the suspension in slowly flowing to stagnant water (slackwater facies *sensu* Bosch & White, 2004). In several places, granite sand was also exposed in artificial floor trenches. Although granite gravels are preserved on the surface near the cave, they are sporadic in the cave. The northern entrance to the cave was dug through the accumulation of allochthonous gravels, predominantly composed of granitic pebbles, with sporadic pebbles of volcanics and quartz sandstone. The gravels were likely deposited on the original terrace surface and redeposited into the collapsed doline-like depression.

The chambers and halls of the cave were almost completely changed by the breakdown (mostly by block and slab breakdown). The ceiling and the walls of the Malužinský dómik Chamber are featured by a vaulted cross-section with step-like dividing planes of breakdown collapses. Large ceiling breakdown cupolas (*sensu* Slabe, 1995) occur in the northern part of the Bociansky banícky dóm Chamber (Figs. 11A and B). They were formed by the gradual flaking of the slabs of thin carbonate beds as a result of the gravitational disintegration of folded carbonates on the cave roof. The floors of the chambers are covered by debris fields, piles of carbonate blocks, and slabs fallen from the ceiling. A similar character of the ceiling can also be observed near entrance no. 2, but in this case, the breakdown is enhanced by the presence of the pervasive fractures oriented NNW-SSE and E-W. In the northern half of the cave, which is formed in layered dolomites, the breakdown and resulting morphologies are more pronounced.

## Interpretation and discussion

### *Tectonic structure of the Hronic Unit*

We believe that the Hronic Unit in the study area comprises two relatively competent tectonic units separated

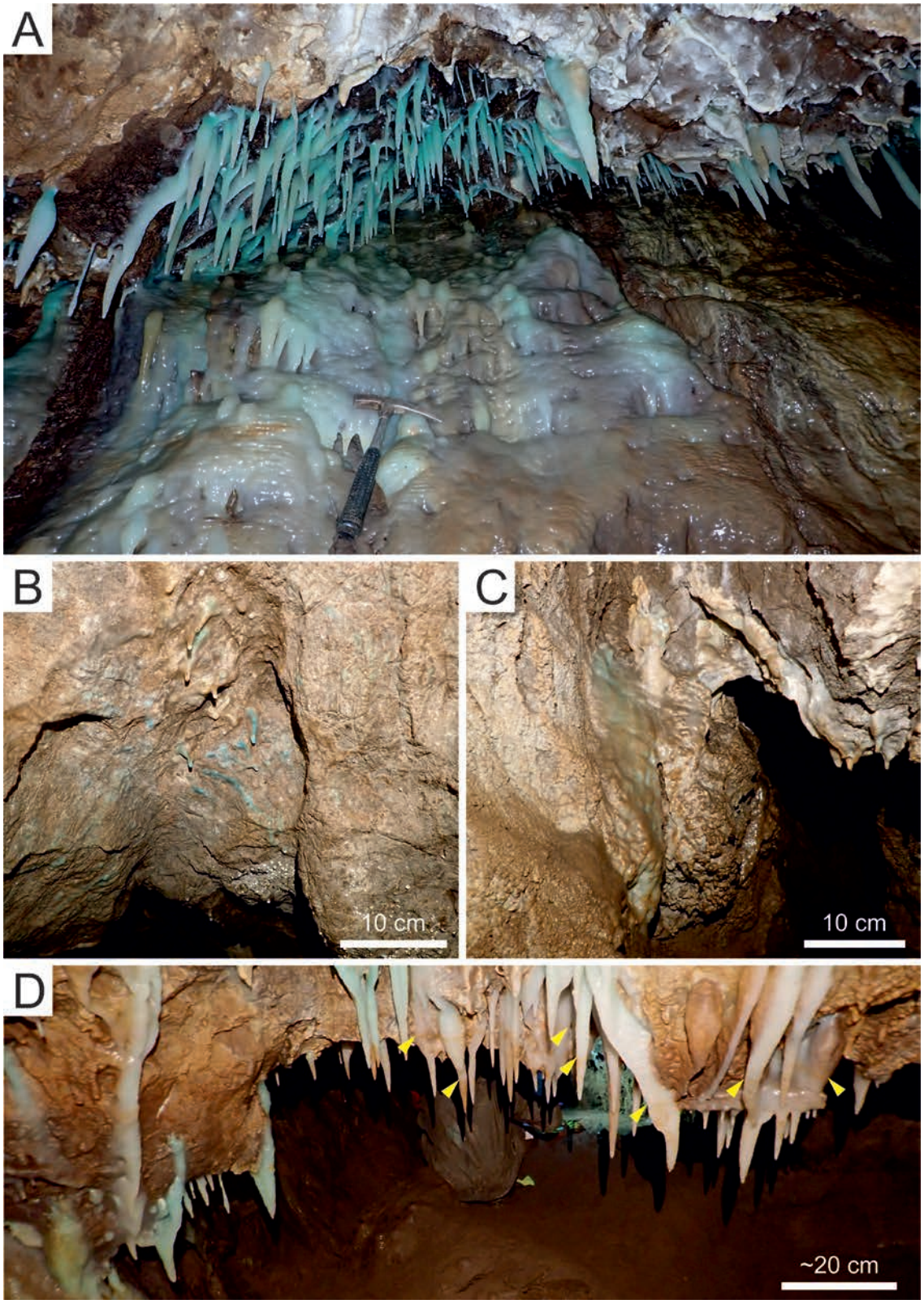


**Fig. 9.** Coloured speleothems of the Blue Cave. **A** – Blue to green dripstones and flowstones in the Sieň modrých šmolkov Hall. **B** – Blue to green speleothems in the passage leading from the entrance nr. 2. **C** – Greenish flowstones in the passage leading from the entrance nr. 1. **D** – Thin veneer of flood sediments deposited on the stalactites in the Sieň modrých šmolkov Hall. Yellow arrows denote the floodmark level of the past flood events. All photos by J. Littva.

by a structurally imbricated zone. The zone involves tectonic slices typically composed of the Permian to Middle Triassic siliciclastic and carbonate rocks (Fig. 1C). The structurally imbricated zone can occasionally involve the Permian volcanics, but they typically form a thick rigid rock package belonging to a competent tectonic unit below the zone (Fig. 1C). The upper competent unit, belonging to the Svarín nappe is predominantly composed of a thick and rigid sequence of the Mesozoic carbonate rocks (Fig. 1C). The structural imbrication likely developed during the translation of the overriding Svarín nappe between two relatively competent and thick rock packages. The carbonates that host the Blue Cave are part of a tectonic slice involved in this zone (compare Figs. 1C and 2A–C). The Čierny Váh carbonates are further internally deformed, as seen from the fold-and-thrust structure found in the Blue Cave (Figs. 5C and 7B), which shows a top-to-the-west shear sense. This movement sense roughly corresponds with the overall northwestern direction of tectonic transport for the Hronic nappes (Biely, 1963; Biely et al., 1997; Kováč & Filo, 1992; Kováč & Havrila, 1998).

In our opinion, the intensively deformed zone between two nappes should not be recognised as a separate nappe. Hence, the separation of three subordinate Hronic nappes as proposed by some authors (Biely, 1963, 1964, p. 28–29, 1976, p. 60–64; Biely et al., 1997, p. 147–149) is not necessary. Instead, it is more plausible to distinguish two subordinate nappes, with the lower nappe forming local imbrications caused by the translation of the overriding nappe. The nappes differ in the facial character of their Middle to Upper Triassic carbonates, with the upper one containing basinal carbonates, which are absent in the lower nappe. On contrary to previous interpretations, which also divided the Hronic Unit into two tectonic units separated by a deformed zone (Biela, 1960, p. 24–27; Biely, 1960, 1962), we consider the structurally imbricate zone to be a local phenomenon. To the west, the zone of imbricated slices becomes progressively thinner and more complicated, until it eventually pinches out. To the east, the rock succession thickens and becomes stratigraphically more coherent, forming a larger, internally less deformed structure (Pukanec duplex *sensu* Tulis & Novotný, 1998, p. 70–71, Appendix 1).

Some authors suggested that the tectonic imbrication could affect the entire body of the lower nappe (e.g., Badár et al., 1965, p. 69–72; Vozár et al., 1983, p. 83–85; Tulis & Novotný, 1998, p. 70–71, Appendix 1). This idea is supported by the occurrence of the slices of the Lower Triassic siliciclastics and the Middle Triassic carbonates below the Paleozoic rocks of the lower nappe (Olšavský, 2007a, b, 2008, p. 168–173). Given the results of our mapping and the rheological considerations, we still believe the rocks above the Permian volcanics are more intensely deformed than the rest of the lower nappe in the study area. Nonetheless, we cannot exclude the existence of other intensely deformed zones situated between the relatively competent rocks of the lower nappe. For example, further to the east, the Middle Triassic Čierny Váh carbonates of the lower nappe are considerably thicker and therefore more rigid. Here, shales, marlstones, and limestones of the Upper Triassic to Cretaceous age seem to be involved in the deformation zone that separates the lower and upper nappes.

Our map generally corresponds with the map of Tulis & Novotný (1998, Appendix 1) better than with the map of Biely et al. (1992), except for the distinct NW-SE fault that is absent in the former map. Although Biely et al. (1992) might have overemphasised the steep faults over thrust faults, this particular fault, also mapped by Vozár et al. (1983), is also recorded in our map (Fig. 2). The right-lateral movement sense on the fault is obvious from the offset in the basal thrust of the upper nappe by approximately 500 meters Hronic Unit (Figs. 1C and 2A). Interestingly, after restoring the offset, mines in the Olovienka Ravine, Malužinská Cave, and the Blue Cave would be located much closer to each other, perhaps even associated with the same thrust fault.

### *Geological controls on the speleogenesis*

Based on the characteristic features, such as dark colour, bedding thickness, and white veins, we consider the Čierny Váh carbonates that host the Blue Cave to be a dolomitised equivalent of the Anisian carbonate formations. The bedded dolomites could be the equivalent of Gutenstein limestones and dolomites, which are typically distinctly bedded (e.g. Moser et al., 2024). The massive dolomites could represent an equivalent of the younger limestone types, which tend to be thick-bedded or massive, such as Annaberg or Steinalm limestones (e.g. Moser & Piros, 2021; Moser et al., 2024). However, massive dolomites might have arisen as a result of a higher degree of dolomitisation, since the process can obliterate bedding (Fig. 11C in Machel, 2004). Our observations in this regard are inconclusive. On the one hand, the micritic microfacies are absent in the massive dolomites (samples MM-1 and MM-2), which would point to a higher degree of recrystallisation. On the other hand, the lower MgO content and preservation of the original textures in the clasts of breccia in the sample MM-7 contradict the idea of the massive dolomites being more dolomitised.

Although limestones to dolomitic limestones are known to be present in the Čierny Váh carbonates (e.g. Urban, 1959; Srnánek, 1962; Badár et al., 1965), the Blue Cave is hosted mainly in the dolomites with high Mg content (Tab. 1). The Mg content above 20 % was also detected in the dolomites that host the nearby Malužinská Cave (Bella et al., 2014). The breccia from the sample

MM-7, taken from the outcrop above the cave entrance, has the MgO content of 18 %, but this rock type was not identified anywhere in the cave. The location of the caves is even more surprising given the presence of both limestones and dolomitic limestones, with MgO content of 2–2.5 % and 15 % respectively, directly in the study area (Urban, 1959). It seems that the MgO content of the Čierny Váh carbonates did not exert a significant control on the formation of the most spacious caves in the study area. As dolomites are typically less prone to for karstification than the limestones, it seems to be facilitated by other factors. Except for the samples MM-5 and MM-7, the dolomite shows little to no intercrystalline porosity. Thus, other porosity types, such as fracture porosity, played a dominant role in the formation of the Blue Cave.

The bedrock structures that predominantly contributed to the formation of the Blue Cave were the brittle tectonic structures (Fig. 6) that developed after the translation of the Hronic nappes. The bedding controls some of the passages in the northeastern part of the cave, but is irrelevant for the southeastern part of the cave that formed in the massive dolomites (Figs. 5A–D and 6). The same is true for the fold-and-thrust structure, which controls the parts of the cave around the Bociansky banícky dóm Chamber, but its influence in other parts of the cave is minimal (Figs. 5A–D and 6). A prominent steep NE-SW fault that predisposes the Malužinský dómik Chamber, separates the cave into two structurally and lithologically distinctive domains (Figs. 5D and 6). The cave spaces between the entrance nr. 2 and the Bociansky banícky dóm Chamber hosted in bedded dolomite seem to be controlled predominantly by the NNW-SSE and E-W fractures (Fig. 6). Southeast of the fault, between the entrance nr. 1 and the Malužinský dómik Chamber, the massive host rock is permeated by two fracture types: (1) NE-SW and (2) NW-SE to NNW-SSE fractures (Fig. 6). Based on the orthogonal orientation of the fracture sets in both domains one could assume that the fractures had originally the same orientation and were rotated into their current position. However, the orientations of fractures associated with blue and green speleothems are consistent across both domains, contradicting the assumption of rotation.

Due to the Triassic age of the host rock and the general absence of kinematic indicators on the brittle structures, attributing the age to the measured brittle structures was challenging. The formation of the fold-and-thrust structure can be quite confidently correlated to the nappe translation, which occurred during the middle part of the Cretaceous (e.g., Plašienka, 2018; Hók et al., 2022). From the other brittle structures, the age could be constrained only for the dextral NE-SW faults, most prominently the distinctive fault crossing the Malužinský dómik Chamber (Figs. 5D, 6, 7C and D). Faults with this kinematics were active only during the E-W compression from the late Paleocene to the middle Eocene (e.g., Pešková et al., 2009; Vojtko et al., 2010; Sůkalová et al., 2012; Gerátová et al., 2022; Hoppanová, 2024). As we did not observe any cross-cutting relationships in the other fracture types, it is not possible to reliably narrow down the age of their activity. A tenuous upper age bracket can be provided by the estimated post-Middle Pleistocene age of speleothems, which are not tectonically disrupted. Hence, at least the fractures that are closely associated with speleothems could not have been active after the speleothem deposition.

### *Source of the green and blue colouration of speleothems*

Based on our results, the hypothesis proposed by Orvošová et al. (2016) for the source of the copper in the blue and green speleothems warrants a modification. The copper mineralisation is indeed known from the Permian rocks, occurring in the sandstones, but also in the barite-sulphide veins of the volcanics (Stankovič in Vozár et al., 1983, pp. 108 – 112). But the Pb-Zn-Cu mineralisation was also detected throughout the Middle Triassic carbonate bedrock in the area, and the presence of copper was reported near the cave (Kantor, 1957; Hanáček, 1963; Biely, 1964; Ivanov et al., 1965; Kantor, 1975; Kantor & Ďurkovičová, 1977). A mineralised zone in the uppermost interval of the borehole Ma-2, located in extreme proximity to the cave, contains chalcopyrite and malachite, and is therefore the most likely copper source. Hence, it is not necessary to derive the copper in the dripwater from the weathering of the ores in the Permian rocks. Although the copper could have been originally remobilised into the Middle Triassic carbonates from the Permian rocks, more research would be required to test this hypothesis. Furthermore, the mineralisation in the carbonates is not evenly disseminated; rather, it seems to be predisposed by the brittle tectonic structures.

The primary sulphide mineralisation seems to be linked to the shallow-dipping thrust faults, while younger supergene copper oxides occur on the steeper NE-SW and NW-SE fractures. Hence, the Pb-Zn mineralisation at the Olovienka Ravine developed during or after mid-Cretaceous nappe stacking. The rock units in the broader area around the Blue Cave experienced episodes of denudation in the Late Cretaceous to the early Eocene and from the Early Miocene to the Holocene (e.g. Danišík et al., 2011; Kováč et al., 2016; Králiková et al., 2016; Vojtko et al., 2016; Kováč et al., 2017). The primary ore could have therefore experienced multiple episodes of oxidising conditions necessary for the formation of malachite and azurite observed in the Blue Cave. One such episode could be dated to be synchronous with the dextral movement on the NE-SW fault during the late Paleocene to the middle Eocene. In other cases, the malachite and azurite appear to be deposited within the preexisting fractures and could be substantially younger than the fractures hosting them.

Notably, the occurrences of azurite and malachite, as well as the blue and green speleothems, seem to be linked to the specific sets of fractures. While the malachite and azurite occur at the NE-SW and NW-SE fractures, the occurrences of blue and green speleothems are limited to the NW-SE-striking fractures. This indicates that despite the difficulties in pinpointing the age of the fractures, the formation of the malachite and azurite is somehow temporally or spatially linked to these fractures. Uncovering this relationship between the minerals and fractures would require more in-depth research that is beyond the scope of this study. The predisposition of the blue and green speleothems on the NW-SE fractures indicates that these fractures represent a main pathway for vadose water that seeps into the cave and forms the speleothems. The fractures probably encounter the same mineralised zone that was drilled in the borehole Ma-2, as they cross the bedrock from the surface to the cave.

### *Origin and development of the cave in relation to the evolution of the valley*

Despite the association of the sulphide ores with the Blue Cave, the predominant morphological features in the cave are consistent with the formation of the cave by meteoric waters, not by sulphuric acid. Nevertheless, the contribution of the supergene sulphuric acid speleogenesis (*sensu* Webb, 2021), i.e. oxidation of sulphide minerals by meteoric waters, cannot be fully ruled out. In the malachite-bearing dolomite collected from the surface, we observed an open vein with rusty brown iron oxides at its edge, covered by euhedral calcite crystals and malachite (Figs. 4E–G). Thus, the vein could have been dissolutionally enlarged before or during the formation of the iron oxides. In the upper interval of the borehole Ma-2 near the cave, the mineralised zone containing chalcopyrite and other sulphide minerals was observed, as well as the indicators of sulphide weathering (Biely, 1964). Biely (1964) noted malachite incrustations, brown vein fillings (likely an oxidised residue after the sulphide weathering) and the porous dolomites (Fig. 3). The chalopyrite oxidation is also believed to occur currently in the bedrock near the cave, playing a crucial role in the formation of blue and green speleothems (Culková et al., 2025). A finely porous dolomite was also observed in the thin section from the sample MM-5 (Figs. 6 and 8D). The sulphide dissolution could have created the sulphuric acid that created or enhanced the porosity of dolomite. This so-called scattered porosity, as described by De Waele et al. (2024), is insufficient to create a cave by itself. But the porosity could have facilitated the subsequent formation of the Blue Cave by enabling easier penetration of aggressive groundwater into the bedrock and increasing the area of the reactive surface. The elevated amounts of Zn in carbonates, likely associated with the sulphide minerals, near the other sizeable Malužiná Cave, further underscores this possibility.

The morphological evidence indicates that the cave was formed chiefly by the aggressive allochthonous waters and repeated floodwater injections from the surface stream into the carbonate bedrock. The position of the cave immediately downstream from the non-karstic rocks also indicates that the waters of the surface stream played a dominant role in the formation of the cave. Prevailing fine-grained slackwater sediments on the cave floor indicate that the cave was formed by slowly flowing stagnant water in phreatic and epiphreatic conditions (i.e. below and at the level of the groundwater table, respectively). This is further supported by the presence of solution facets (Fig. 10B), which indicate that fine-grained sediments were deposited in the cave during its formation. Morphological forms that would indicate a faster water flow, like smaller scallops, are absent.

The primary phase of the cave evolution probably occurred in a phreatic zone during the formation of a flat rock surface of the upper stream terraces above the cave. The extensive occurrence of phreatic morphological forms in the cave (Fig. 10A) contrasts with the almost complete absence of distinctive epiphreatic and vadose forms (horizontal wall notches, floor channels). This suggests that the most extensive speleogenesis occurred mainly below the level of the surface stream, and in later stages, the cave was only partially remodelled.

After the incision of the valley floor, the cave was remodelled during the formation of middle and lower stream terraces, as the surface water sporadically penetrated into the cave located at the left bank of the surface streambed. Allochthonous water entered the cave through several small swallets and opened fissures that occurred on the inside convex bank of the meandering stream, mostly during floods (bank storage *sensu* Palmer, 1991, 2007). Inflow conduits leading downwards from these inlets were interconnected in the adjacent southeastern part of the cave, creating a network pattern. The limited capacity of the inlets prevented a greater amount of coarse-grained sediments from the surface streambed from being transported into the cave. The solution facets associated with the deposition of the fine-grained sediments (Fig. 10B), as well as thin sediment veneers on stalactites (Fig. 9D), were also formed in this stage. Air traps at the top of the ceiling pockets (Fig. 10E) provide additional evidence of the former flooding of the cave, suggesting that passages were occasionally filled with water under pressure during repeated floods. During the vadose development phase, fine-grained sediments were partially removed from the cave by moderate-flowing water. In elevated areas, the cave bedrock floor could have been slightly lowered.

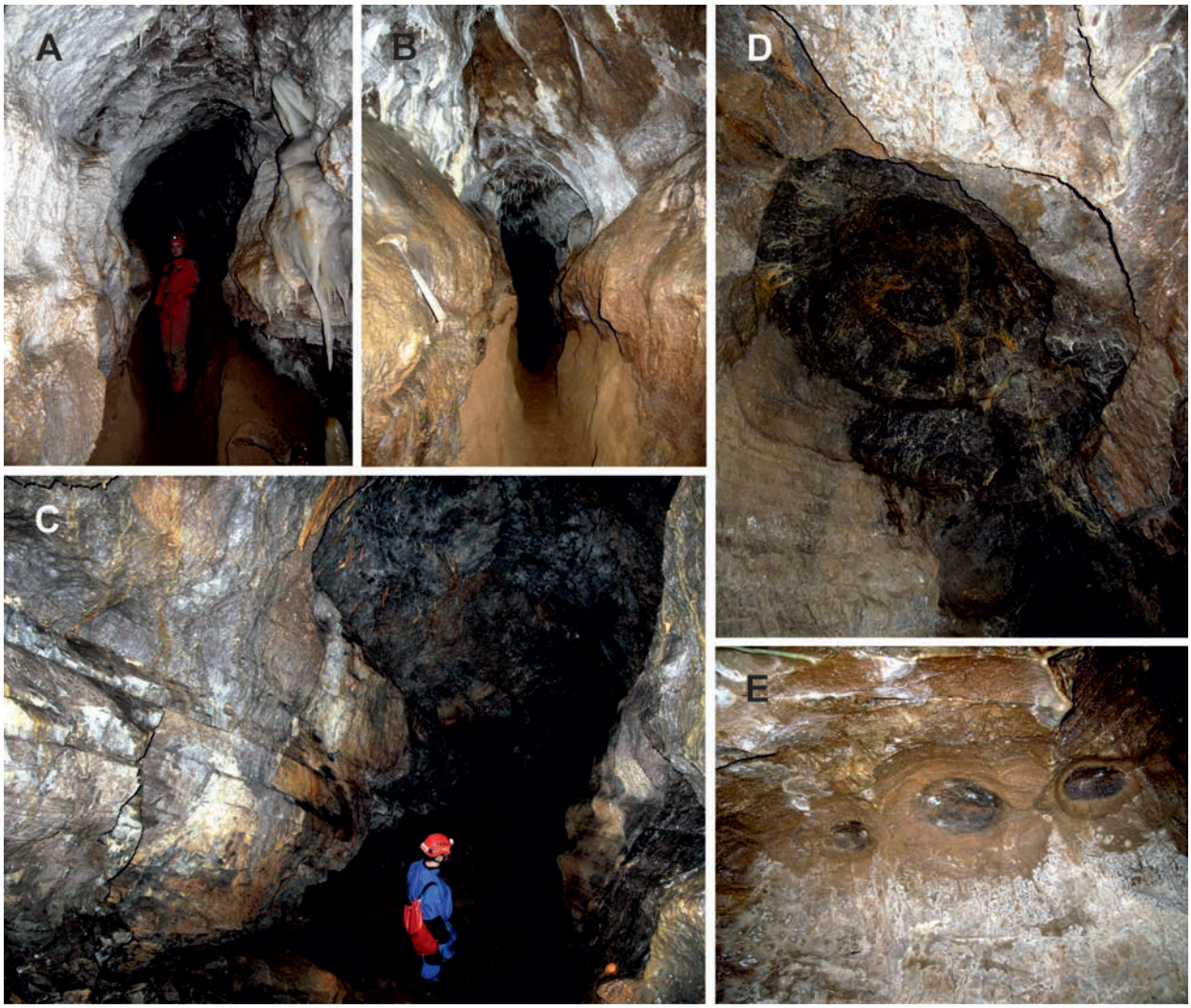


**Fig. 10.** Solution morphologies in the cave. **A** – Phreatic passage controlled by steep fracture. **B** – Inwardly sloping solution facets (planes of repose) on both sides of phreatic passage controlled by steep fracture. **C** – Multi-phase passage consisting of phreatic tube and lower epiphreatic to vadose incised floor (partly remodelled by breakdown). **D** – Large ceiling pocket. **E** – Air traps at the top of the ceiling pockets. All photos by P. Bella.

In the final stage of cave evolution, phreatic solution morphologies were remodelled by breakdown, mostly in places of increased structural and tectonic disintegration of the bedrock.

The main parts of the cave span relative heights of 20–25 m above the current Boca Stream's surface streambed, which correspond to the relative heights of the upper terraces. In the study area, the upper terraces are the most extensive of the mapped terraces and occur both upstream and downstream from the cave. The distinctive river terrace at almost the same relative height (about 20 m) above the recent streambed occurs on the left side of the Váh River valley between the village of Kráľova Lehota and the town of Liptovský Hrádok (Hromádka, 1931; Kettner & Šťastný, 1931; Vitásek, 1932). Compared with the relative height and estimated age of river terraces further downstream in the Liptovská kotlina Basin (Droppa, 1964, 1970, 1972c; Vitovič & Minár, 2018), and cave levels in the Demänovská dolina and Jánska dolina valleys (e.g. Droppa, 1966, 1972a, b), it can be assumed that the Blue Cave formation initiated during the Middle Pleistocene.

The surface of the upper terraces is perturbed by karst collapse processes. Several collapsed doline-like depressions with numerous granitic pebbles on the bottom, can be observed on the upper terraces (Fig. 2A). They formed due to the higher degree of karstification of the carbonate bedrock below the stream terrace and both cave entrance were excavated in these depressions (Fig. 2A). Comparable, albeit less distinctive depressions with

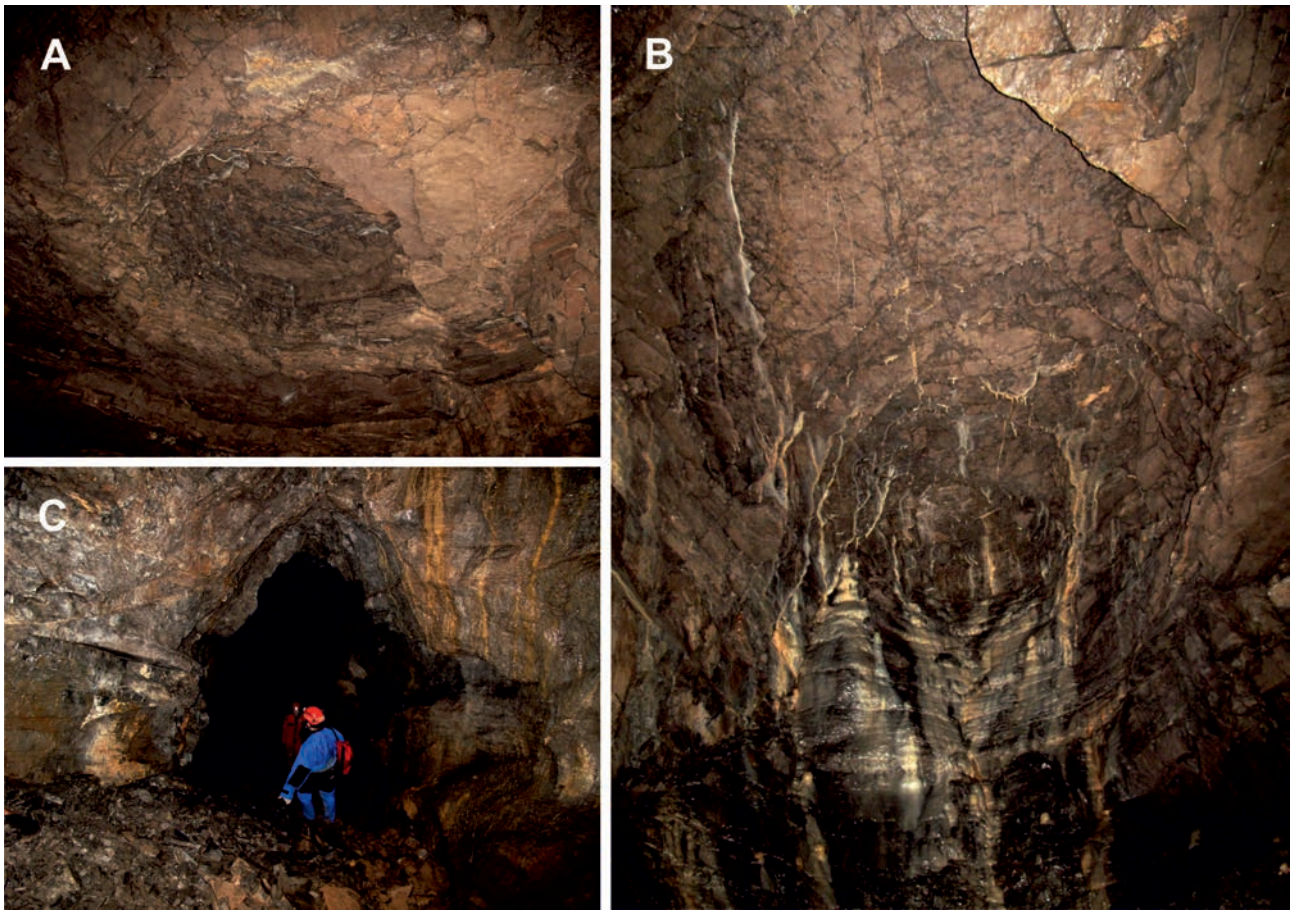


**Fig. 11.** Breakdown cave morphologies. **A**, **B** – Shallow breakdown cupolas. **C** – Phreatic passage partly remodelled by breakdown, its original floor is covered by debris. All photos by P. Bella.

granitic gravels can be observed on the volcanic bedrock. Assuming the depressions are not anthropogenic, they could be caused by the presence of the karstified Triassic carbonate rocks underthrust below the Permian volcanics.

### *Utilising the caves in geological research*

The observation of several key geological phenomena would not be possible without direct observations of the bedrock in the Blue Cave. For example, the bedded dolomites and geological structures observed in the cave were not observed in the surface mapping. While the malachite was observed in the talus of the surface outcrop, the malachite and azurite in the cave could be observed more clearly and in their original context (compare Figs. 4E–G with Figs. 7E–H). Although important insights were also gleaned from the borehole data, they are much costlier than the observations on the rocky cave walls. Our findings underscore the utility of the caves as a sort of 'natural boreholes' in the geological research (cf. Vlček, 2011; Šebela et al., 2021).

## Conclusions

Based on the geological mapping of the Blue Cave's surroundings, the Middle Triassic carbonates that host the cave are strongly perturbed by the mid-Cretaceous stacking of the Hronic nappes. We propose that the Hronic Unit in the study area is separated into two nappes, with the carbonates located atop of the lower nappe perturbed by an array of imbricated thrusts. One such thrust plane hosts the Pb-Zn-Cu mineralisation, which is either coeval with the thrusting or postdates it. Subsequently, the nappe stack was disrupted by the younger generations of steeper brittle structures, with some of them being mineralised by malachite and azurite. The dextral NE-SW faults can be dated to the late Paleocene – middle Eocene, based on the paleostress studies (e.g., Pešková et al., 2009; Vojtko et al., 2010; Sůkalová et al., 2012; Gerátová et al., 2022). The age of the other brittle structures could not be constrained to a reasonably narrow timeframe. As the malachite and azurite form by oxidation of primary ores in the near-surface conditions, their formation should record

denudation events of the Hronic Unit. Such denudation events are possible either from the Late Cretaceous to the early Eocene or from the Early Miocene to the Holocene (Danišík et al., 2011; Kováč et al., 2016, 2017; Králiková et al., 2016; Vojtko et al., 2016).

The high MgO content of the host rock (> 20 %), despite the presence of dolomitic limestones and even limestones in the study area, suggests that the purity of the host rock played a limited role in the cave formation. The cave spaces formed and enlarged along the four types of fracture sets with the following orientations: (1) NE-SW, (2) NNW-SSE to NW-SE, (3) NNE-SSW, and (4) E-W. Although the presence of Pb-Zn sulphide ores can be associated with the unusual cave types formed by the sulphuric acid, there is no evidence that the Blue Cave was created by such a mechanism. Our findings caution against premature attribution of the cave types based purely on the presence of Pb-Zn sulphide ores in carbonate bedrock. Nevertheless, the carbonates in the cave and near the cave contain several clues pointing to the initial enhancement of the bedrock porosity by the sulphide dissolution. The borehole Ma-1 drilled near the cave (Biely, 1964) encountered sulphide minerals and products of their oxidation in its uppermost interval. Moreover, the porous dolomites were also noted in this mineralised zone, their porosity possibly created by the sulphuric acid produced by the sulphide oxidation. Dolomites with fine pores were also observed in the sample MM-5 from the cave. Although this interaction did not directly lead to the formation of the cave, the emergence of the porosity could have been a precursor step for the subsequent formation of the Blue Cave.

Based on the morphological evidence, we propose the Blue Cave was formed predominantly by the aggressive allochthonous waters from the surface stream in three main stages. In Stage I, the phreatic passages developed below the water table during the formation of the stream terrace that presently occurs above the cave. Stage II was marked by the stream downcutting interrupted by the episodic formation of the younger terraces. During this stage, the growth of blue and green speleothems initiated and the cave was periodically flooded, as evidenced by the epiphreatic morphologies and flood sediment veneer covering the lower parts of the stalagmites. Stage III is marked by the collapse and breakdown processes, which significantly remodelled the parts of the cave that are located closest to the surface, namely the entrance parts and the Bociansky banícky dóm Chamber. Based on the relative height of the terrace above the Blue Cave and its comparison with the more extensive river terraces downstream, the estimated age for the terrace is the Middle Pleistocene. Consequently, we estimate a similar age for the initial formation of parts of the Blue Cave, as well as the subsequent initial deposition of some of the blue and green speleothems.

The blue and green colouration of speleothems in the Blue Cave was previously attributed to the copper sourced from the weathering of the Permian rocks neighbouring the cave's Middle Triassic carbonate host rock (Orvošová et al., 2016). However, a discovery of the little-known works that describe the Pb-Zn-Cu mineralisation directly from the carbonate host rock (Kantor, 1957; Hanáček, 1963; Biely, 1964; Ivanov et al., 1965; Kantor, 1977) led us to pursue an alternative hypothesis. Based on the digitised data from these works, in combination with our field data, we propose that the copper is sourced directly from the carbonates that host the cave. The copper most likely originates from the mineralised zone containing chalcopyrite and malachite drilled in the uppermost part of the borehole Ma-2 (Biely, 1964), located approximately 130 m from the cave. The observations from the cave suggest that the zone was intersected by the NE-SW and NW-SE fractures, which host the malachite and azurite. Following the cave formation, the copper was incorporated into blue and green speleothems, albeit these formed only on the NW-SE-striking fractures.

The study of the rock walls in the Blue Cave enabled the observation of geological features that could not be observed on the surface. This work thus underscores the fact that the geological study of the caves can be a useful method in elucidating the local geology. The presented new knowledge about the Blue Cave is also important for its protection as a natural monument (according to the Nature and Landscape Protection Act No. 543/2002 Coll. as amended). The cave occurs in the territory of the Nízke Tatry National Park, but near a frequent road leading through the Čertovica mountain pass. Moreover, a side field roads lead near and above the cave to the adjacent meadow and forest, as well as to several cottages. Several parts of this later discovered cave are located shallowly (at least about 5 m) below the terrain surface. The surface area above the cave does not have a higher level of nature protection than the surrounding part of the national park without caves. The buffer zone of the cave should be considered to prevent the artificial changes of the surface landforms, the deforestation of the surface above the cave, the building of recreational facilities or any other unacceptable human activities in the catchment area of the cave.

## Acknowledgements

The geological and geomorphological research presented here was supported by institutional funding from the State Nature Conservancy of the Slovak Republic, the Slovak Caves Administration in Liptovský Mikuláš and the Grant Agency of Slovak Republic (VEGA) under the project no. 1/0323/24. We would like to thank J. Šmoll and G. Majerníčková from the Slovak Speleological Society, and L. Dušeková and P. Staník from the Slovak Caves

Administration for their assistance during the fieldwork. We are also grateful for the comments and remarks from reviewers Peter Šottník and Mário Olšavský, which substantially improved our paper.

## References


Badár, J., Novotný, L., Reimont, V. & Švábl, E., 1965: Zpráva ku geologickej mape z lokality Čierny Váh z oblasti Nižná Boca – Liptovská Teplička. Spišská Nová Ves, Geologický prieskum uránového priemyslu. *Manuscript. Bratislava, Archive of St. Geol. Inst. of D. Štúr* (arch. no. 55175), 99 pp.

Bella, P., Littva, J., Pruner, P., Gaál, Ľ., Bosák, P. & Haviarová, D., 2014: Malužinská jaskyňa v severovýchodnej časti Nízkych Tatier: freatická speleogenéza spôsobená vodami vystupujúcimi pozdĺž zlomovej zóny. *Slovenský kras*, 52, 2, 111 – 126.

Biela, A., 1960: Geologické pomery územia na sútoku Bieleho a Čierneho Váhu. Master's Thesis. Katedra geológie a paleontológie, Prírodovedecká fakulta Univerzity Komenského. *Manuscript. Bratislava, Archive of St. Geol. Inst. of D. Štúr* (arch. no. 81079), 53 pp.

Biely, A., 1960: Chočský príkrov na severných svahoch Nízkych Tatier. *Geologické práce, Zprávy*, 20, 127 – 134.

Biely, A., 1962: Niekoľko tektonických a stratigraficko-litologických poznatkov z východnej časti Nízkych Tatier a Tribča. *Geologické práce, Zošit*, 62, 205 – 218.

Biely, A., 1963: Beitrag zur Kenntnis der inneren Baues der Choč-Einheit. *Geologické práce, Zprávy,* 28, 69 – 78.

Biely, A., 1964: Výskum mezozoika v Nízkych Tatrách, list Horná Lehota, ročná správa za rok 1963. *Manuscript. Bratislava, Archive of St. Geol. Inst. of D. Štúr* (archive no. 12924), 35 pp.

Biely, A., 1976: Vysvetlivky k mezozoiku S svahov Nízkych Tatier – východná časť. *Manuscript. Bratislava, Archive of St. Geol. Inst. of D. Štúr* (archive no. 38208), 72 pp.

Biely, A., Beňuška, P., Bezák, V., Bujnovský, A., Halouzka, R., Ivanička, J., Kohút, M., Klinec, A., Lukáčik, E., Maglay, J., Miko, O., Pulec, M., Putiš, M. & Vozár, J., 1992: Geologická mapa Nízkych Tatier 1 : 50 000 [map]. *Bratislava, Geologický ústav Dionýza Štúra*.

Biely, A., Bezák, V., Bujnovský, A., Vozárová, A., Klinec, A., Miko, O., Halouzka, R., Vozár, J., Beňuška, P., Hanzel, V., Kubeš, P., Liščák, P., Lukáčik, E., Maglay, J., Molák, B., Pulec, M., Putiš, M. & Slavkay, M., 1997: Vysvetlivky ku geologickej mape Nízkych Tatier. *Bratislava, Geologická služba Slovenskej republiky, Vydavateľstvo Dionýza Štúra*, 232 pp.

Bosch, R. F. & White, W. B., 2004: Lithofacies and Transport of Clastic Sediments in Karstic Aquifers. In: Sasowsky, I. D. & Mylroie, J. (eds.): Studies of Cave Sediments. *Boston, MA, Springer US*, 1 – 22. https://doi.org/10.1007/978-1-4419-9118-8_1.

Bretz, J. H., 1942: Vadose and Phreatic Features of Limestone Caverns. *The Journal of Geology*, 50, 6, 675 – 811.

Culková, E., Bellová, R., Littva, J., Bella, P. & Tomčík, P., 2025: Detection of copper in blue-green stalactites using a bare boron doped diamond electrode: Clean and sustainable sensing platform for cave samples analysis. *Microchemical Journal*, 218, 115806. https://doi.org/10.1016/j.microc.2025.115806.

Čechovič, V., 1942: Zpráva o prieskumu barytových ložísk v okolí Malužinej. Handlová, Ústřední ústav geologický. *Manuscript. Bratislava, Archive of St. Geol. Inst. of D. Štúr* (archive no. 8156), 7 pp.

Chovan, M., Slavkay, M. & Michálek, J., 1996: Ore mineralization of the Ďumbierske Tatry Mts. (Western Carpathians, Slovakia). *Geologica Carpathica*, 47, 6, 371 – 382.

CloudCompare, 2023: v2.13.1. Available at: http://www.cloudcompare.org/.

Danišík, M., Kadlec, J., Glotzbach, C., Weisheit, A., Dunkl, I., Kohút, M., Evans, N. J., Orvošová, M. & McDonald, B. J., 2011: Tracing metamorphism, exhumation and topographic evolution in orogenic belts by multiple thermochronology: a case study from the Nízke Tatry Mts., Western Carpathians. *Swiss Journal of Geosciences*, 104, 2, 285 – 298. https://doi.org/10.1007/s00015-011-0060-6.

De Waele, J., D'Angeli, I. M., Audra, P., Plan, L. & Palmer, A. N., 2024: Sulfuric acid caves of the world: A review. *Earth-Science Reviews*, 250, 104693. https://doi.org/10.1016/j.earscirev.2024.104693.

Droppa, A., 1964: Výskum terás Váhu v strednej časti Liptovskej kotliny. *Geografický časopis*, 16, 4, 313 – 325.

Droppa, A., 1966: The correlation of some horizontal caves with river terraces. *Studies in Speleology*, 1, 186 – 192.

Droppa, A., 1970: Výskum riečnych terás v zátopovej oblasti Liptovská Mara. *Vlastivedný zborník Liptov*, 1, 7 – 34.

Droppa, A., 1972a: Geomorfologické pomery Demänovskej doliny. *Slovenský kras*, 10, 9 – 46.

Droppa, A., 1972b: Krasové javy Jánskej doliny na severnej strane Nízkych Tatier. *Československý kras*, 21, 73 – 96.

Droppa, A., 1972c: Výskum riečnych terás v okolí Ružomberka. *Vlastivedný zborník Liptov*, 2, 11 – 25.

Ewers, R. O., 1966: Bedding-Plane Anastomoses and Their Relation to Cavern Passages. *Bulletin of the National Speleological Society*, 28, 3, 133 – 140.

Farrant, A. R. & Smart, P. L., 2011: Role of sediment in speleogenesis; sedimentation and paragenesis. *Geomorphology*, 134, 1, Geomorphology and Natural Hazards in Karst Areas, 79 – 93. https://doi.org/10.1016/j.geomorph.2011.06.006.

Ford, D. C., 1977: Genetic classification of solution cave system. In: Ford, T. D. (ed.): Proceeding of the 7th International Congress of Speleology. Sheffield, 10 – 17 September 1977, *International Union of Speleology British Cave Research Association*, 189 – 192.

Ford, D. C., 1988: Characteristics of Dissolutional Cave Systems in Carbonate Rocks. In: James, N. P. & Choquette, P. W. (eds.): Paleokarst. *New York – Berlin – Heidelberg – London – Paris – Tokyo, Springer*, 25 – 57. https://doi.org/10.1007/978-1-4612-3748-8_2.

Ford, D. C., 2000: Speleogenesis under unconfined settings. In: Klimchouk, A. B., Ford, D. C. & Palmer, A. N. (eds.): Speleogenesis. Evolution of Karst Aquifers. *Huntsville, Alabama, U. S. A., National Speleological Society*, 319 – 324.

Ford, D. C. & Ewers, R. O., 1978: The development of limestone cave systems in the dimensions of length and depth. *Canadian Journal of Earth Sciences*, 15, 11, 1 783 – 1 798. https://doi.org/10.1139/e78-186.

Gerátová, S., Vojtko, R., Lačný, A. & Kriváňová, K., 2022: The structural pattern and tectonic evolution of the Muráň fault revealed by geological data, fault-slip analysis, and paleostress reconstruction (Western Carpathians). *Geologica Carpathica*, 73, 1, 43 – 62. https://doi.org/10.31577/GeolCarp.73.1.3.

Hanáček, J., 1963: Ročná správa o geochemickom výskume karbonatických hornín v okolí Malužinej. *Manuscript. Bratislava, Archive of St. Geol. Inst. of D. Štúr* (archive no. 11358), 15 pp.

Havrila, M., 2011: Hronikum: paleogeografia a stratigrafia (vrchný pelsón – tuval), štrukturalizácia a stavba. *Geologické práce, Správy*, 117, 7 – 103.

Heeb, B., 2020: Paperless Cave Surveying. Available at: https://paperless.bheeb.ch/index.html.

Hók, J., Schuster, R., Pelech, O., Vojtko, R. & Šamajová, L., 2022: Geological significance of Upper Cretaceous sediments in deciphering of the Alpine tectonic evolution at the contact of the Western Carpathians, Eastern Alps and Bohemian Massif. *International Journal of Earth Sciences*, 111, 1 805 – 1 822. https://doi.org/10.1007/s00531-022-02201-5.

Hoppanová, E., 2024: Cu-Sb-As mineralizácia v karbonátových brekciách styku hronika a veporika pri Brezne: štruktúrne pomery a alterácia hostiteľských hornín. Rigorosum Thesis. *Manuscript. Banská Bystrica, Univerzita Mateja Bela v Banskej Bystrici, Fakulta prírodných vied*, 119 pp. Available at: https://opac.crzp.sk/?fn=detailBiblioForm&sid=53EEEDF946F250FB448F2DA3B71B.

Howard, A. D., 1971: Quantitative measures of cave patterns. *Caves and Karst*, 13, 1, 1 – 7.

Hromádka, J., 1931: Povrchové formy Slovenska a jejich výskum. *Časopis učenej spoločnosti P. J. Šafárika,* 5, 3, 484 – 510.

Ilavský, J. & Ilavská, Ž., 1949: Zpráva o prieskume výskytov barytu pri Malužinej. Spišská Nová Ves, Železnorudné bane. *Manuscript. Bratislava, Archive of St. Geol. Inst. of D. Štúr* (archive no. 3397), 4 pp.

Ivanov, M., Hanáček, J. & Biely, A., 1965: Geochemický výskum metasomatických zrudnení v karbonátových horninách centrálnej časti Karpát. *Manuscript. Bratislava, Archive of St. Geol. Inst. of D. Štúr* (archive no. 15687), 201 pp.

Jeremenko, D., 1956: Malužiná – Svidovo – ložiskový list č. 113 – melafýr a porfyrický melafýr. Trenčín, Nerudný prieskum. *Manuscript. Bratislava, Archive of St. Geol. Inst. of D. Štúr* (archive no. 2112), 34 pp.

Kantor, J., 1957: Zpráva o geochemickej prospekcii na olovo v Nízkych Tatrách. *Manuscript. Bratislava, Archive of St. Geol. Inst. of D. Štúr* (archive no. 2555), 11 pp.

Kantor, J., 1975: Izotopy síry na Pb-Zn ložiskách z mezozoických karbonátov Západných Karpát. *Manuscript. Bratislava, Archive of St. Geol. Inst. of D. Štúr* (archive no. 35637), 181 pp.

Kantor, J., 1977: Pb-Zn-Ores of the Westcarpathian Triassic and the Distribution of Their Sulphur Isotopes. In: Klemm, D. D. & Schneider, H.-J. (eds.): Time- and Strata-Bound Ore Deposits. *Berlin – Heidelberg, Springer*, 294 – 304. https://doi.org/10.1007/978-3-642-66806-7_19.

Kantor, J. & Ďurkovičová, J., 1977: Izotopy síry na barytových ložiskách Západných Karpát. *Manuscript. Bratislava, Archive of St. Geol. Inst. of D. Štúr* (archive no. 2555), 237 pp.

Kettner, R. & Šťastný, V., 1931: Geologická mapa severního svahu Nízkých Tater v okolí Liptovského Hrádku [map]. *Praha, Knihovna Statního ústavu geologického Československé republiky; 13, A. Vojenský zeměpisný ústav*.

Kováč, M., Márton, E., Oszczypko, N., Vojtko, R., Hók, J., Králiková, S., Plašienka, D., Klučiar, T., Hudáčková, N. & Oszczypko-Clowes, M., 2017: Neogene palaeogeography and basin evolution of the Western Carpathians, Northern Pannonian domain and adjoining areas. *Global and Planetary Change*, 155, 133 – 154. https://doi.org/10.1016/j.gloplacha.2017.07.004.

Kováč, M., Plašienka, D., Soták, J., Vojtko, R., Oszczypko, N., Less, G., Ćosović, V., Fügenschuh, B. & Králiková, S., 2016: Paleogene palaeogeography and basin evolution of the Western Carpathians, Northern Pannonian domain and adjoining areas. *Global and Planetary Change*, 140, 9 – 27. https://doi.org/10.1016/j.gloplacha.2016.03.007.

Kováč, P. & Filo, I., 1992: Structural interpretation of the Choč nappe outliers of the Chočské vrchy Mts. *Mineralia Slovaca,* 24, 1 – 2, 39 – 44.

Kováč, P. & Havrila, M., 1998: Inner structure of Hronicum. *Slovak Geological Magazine*, 4, 4, 275 – 280.

Králiková, S., Vojtko, R., Hók, J., Fügenschuh, B. & Kováč, M., 2016: Low-temperature constraints on the Alpine thermal evolution of the Western Carpathian basement rock complexes. *Journal of Structural Geology*, 91, 144 – 160. https://doi.org/10.1016/j.jsg.2016.09.006.

Kubáň, T., 1956: Správa o základnom inžiniersko-geologickom výskume pre údolnú priehradu Malužiná na rieke Boca v Liptove. *Manuscript. Bratislava, Archive of St. Geol. Inst. of D. Štúr* (archive no. 3171), 17 pp.

Lange, A., 1963: Planes of repose in caves. *Cave Notes*, 5, 6, 41 – 48.

Lauritzen, S.-E. & Lundberg, J., 2000: Solutional and erosional morphology. In: Klimchouk, A. B., Ford, D. C., Palmer, A. N. & Dreybrodt, W. (eds.): Speleogenesis. Evolution of Karst Aquifers. *Huntsville, Alabama, U.S.A., National Speleological Society*, 408 – 426.

Lexa, J., Bezák, V., Elečko, M., Mello, J., Polák, M., Potfaj, M. & Vozár, J., 2000: Geologická mapa Západných Karpát a priľahlých území [map]. Scale 1 : 500 000. *Bratislava, Ministerstvo životného prostredia Slovenskej republiky, Štátny geologický ústav Dionýza Štúra.*

Lošonská, M., 1984: Plynovod Malužiná. Liptovský Hrádok, Agrostav. *Manuscript. Bratislava, Archive of St. Geol. Inst. of D. Štúr* (archive no. 57054), 13 pp.

Machel, H. G., 2004: Concepts and models of dolomitization: a critical reappraisal. In: Braithwaite, C. J. R., Rizzi, G. & Darke, G. (eds.): The Geometry and Petrogenesis of Dolomite Hydrocarbon Reservoirs. *Geological Society of London*, 0. https://doi.org/10.1144/GSL.SP.2004.235.01.02.

Moser, M. & Piros, O., 2021: Lithostratigraphic definition of the Anisian carbonate-ramp deposit of the Annaberg Formation (Middle Triassic, Northern Calcareous Alps, Austria). *Geologica Carpathica*, 72, 3, 173 – 194. https://doi.org/10.31577/GeolCarp.72.3.1.

Moser, M., Wagreich, M. & Piros, O., 2024: The type-section of the Gutenstein Formation at Gutenstein revisited (Anisian, Northern Calcareous Alps, Lower Austria): Lithostratigraphy, biostratigraphy and regional overview. *Austrian Journal of Earth Sciences*, 117, 1, 113 – 147. https://doi.org/10.17738/ajes.2024.0008.

Mudrák, S. & Budaj, M., 2010: The Therion Book. *Distributed under the GNU General Public License*, 108 pp. Available at: https://github.com/therion/therion/releases/download/v6.3.4/thbook-v6.3.4.pdf.

Olšavský, M., 2007a: Spodný trias na báze bocianskeho čiastkového príkrovu hronika (Nízke Tatry, na JV od Liptovskej Tepličky, Rovienky). *Mineralia Slovaca*, 39, 1, *Geovestník*, 19 – 20.

Olšavský, M., 2007b: Stavba hronika na severovýchodných svahoch Nízkych Tatier. *Mineralia Slovaca*, 39, 4, *Geovestník*, 12.

Olšavský, M., 2008: Faciálna analýza depozičných sekvencií maluzinského súvrstvia a jeho geologická stavba na SV svahoch Nízkych Tatier. Doctoral Thesis. *Manuscript. Bratislava, Prírodovedecká fakulta Univerzity Komenského*, 194 pp. Available at: https://www.researchgate.net/publication/321383024_Facialna_analyza_depozicnych_sekvencii_maluzinskeho_suvrstvia_a_jeho_geologicka_stavba_na_SV_svahoch_Nizkych_Tatier.

Orvošová, M., Milovská, S., Mikuš, T., Šmoll, J., Majerníčková, G. & Karošiak, I., 2016: Sintre zafarbené kovovými iónmi v Modrej jaskyni, Nízke Tatry, Slovensko. *Slovenský kras*, 54, 2, 131 – 138.

Palmer, A. N., 1991: Origin and morphology of limestone caves. *Geological Society of America Bulletin*, 103, 1, 1 – 21. https://doi.org/10.1130/0016-7606(1991)103<0001:OAMOLC>2.3.CO;2.

Palmer, A. N., 2007: Cave Geology. *Dayton, Ohio, Cave Books*, 454 pp.

Pešková, I., Vojtko, R., Starek, D. & Sliva, Ľ., 2009: Late Eocene to Quaternary deformation and stress field evolution of the Orava region (Western Carpathians). *Acta Geologica Polonica*, 59, 1, 73 – 91.

Plašienka, D., 2018: Continuity and Episodicity in the Early Alpine Tectonic Evolution of the Western Carpathians: How Large-Scale Processes Are Expressed by the Orogenic Architecture and Rock Record Data. *Tectonics*, 37, 7, 2 029 – 2 079. https://doi.org/10.1029/2017TC004779.

Pristašová, L., 2024: Teplota vzduchu v Maluzinskej a Modrej jaskyni v Nízkych Tatrách. *Aragonit*, 29, 2, 61 – 67.

QGIS Development Team, 2024: QGIS Geographic Information System, 3.34. Available at: https://www.qgis.org.

Röller, K. & Trepmann, C. A., 2003: Stereo32, Version 1.0.1.

Slabe, T., 1995: Cave Rocky Relief and its Speleogenetical Significance. *Ljubljana, ZRC SAZU, Založba ZRC*, 128 pp. https://doi.org/10.3986/961618203X.

Srnánek, J., 1962: Inžiniersko-geologická štúdia údolia Čierneho Váhu. Riaditeľstvo vodohospodárskeho rozvoja. *Manuscript. Bratislava, Archive of St. Geol. Inst. of D. Štúr* (archive no. 11118), 36 pp.

Sůkalová, Ľ., Vojtko, R. & Pešková, I., 2012: Cenozoic deformation and stress field evolution of the Kozie chrbty Mountains and the western part of Hornád Depression (Central Western Carpathians). *Acta Geologica Slovaca*, 4, 1, 53 – 64.

Šebela, S., Stemberk, J. & Briestenský, M., 2021: Microdisplacement monitoring in caves at the Southern Alps-Dinarides-Southwestern Pannonian Basin junction. *Bulletin of Engineering Geology and the Environment*, 80, 10, 7 591 – 7 611. https://doi.org/10.1007/s10064-021-02382-4.

Šmoll, J., 2017: The Modrá Cave (The Blue Cave) in the Low Tatra Mts. *Bulletin of the Slovak Speleological Society, Issued for the purpose of the 17th Congress of the IUS, Sydney 2017*, 66 – 68.

Thiele, S. T., Grose, L., Samsu, A., Micklethwaite, S., Vollgger, S. A. & Cruden, A. R., 2017: Rapid, semi-automatic fracture and contact mapping for point clouds, images and geophysical data. *Solid Earth*, 8, 6, 1 241 – 1 253. https://doi.org/10.5194/se-8-1241-2017.

Tulis, J. & Novotný, L., 1998: Zhodnotenie geologických prác na U rudy v mladšom paleozoiku hronika v severnej časti Nízkych Tatier a Kozích chrbtov. *Manuscript. Bratislava, Archive of St. Geol. Inst. of D. Štúr* (archive no. 82752), 144 pp.

Urban, F., 1959: Průzkum kamene v ČSR 1959, Malužiná. Brno, Geologický průzkum. *Manuscript. Bratislava, Archive of St. Geol. Inst. of D. Štúr* (archive no. 8388), 19 pp.

Vitásek, F., 1932: Terasy horního Váhu. A, 4. *Brno, Spisy odboru Československé spoločnosti zeměpisné v Brně*, 23 pp.

Vitovič, L. & Minár, J., 2018: Morphotectonic analysis for improvement of neotectonic subdivision of the Liptovská kotlina Basin (Western Carpathians). *Geografický časopis*, 70, 3, 197 – 216. https://doi.org/10.31577/geogrcas.2018.70.3.11.

Vlček, L., 2011: Geologická stavba severných svahov Ďumbierskych Tatier a jej vplyv na tvorbu krasového fenoménu. Doctoral Thesis. *Manuscript. Bratislava, Univerzita Komenského v Bratislave*, 168 pp.

Vojtko, R., Králiková, S., Jeřábek, P., Schuster, R., Danišík, M., Fügenschuh, B., Minár, J. & Madarás, J., 2016: Geochronological evidence for the Alpine tectonothermal evolution of the Veporic Unit (Western Carpathians, Slovakia). *Tectonophysics*, 666, 48 – 65. https://doi.org/10.1016/j.tecto.2015.10.014.

Vojtko, R., Tokárová, E., Sliva, Ľ., Pešková, I. & Sliva, Ľ., 2010: Reconstruction of Cenozoic paleostress fields and revised tectonic history in the northern part of the Central Western Carpathians (the Spišská Magura and Východné Tatry Mountains). *Geologica Carpathica*, 61, 3, 211 – 225. https://doi.org/10.2478/v10096-010-0012-5.

Vozár, J., 1970: Výskum permských vulkanitov Chočského príkrovu na severných svahoch Nízkych Tatier – západná časť. *Manuscript. Bratislava, Archive of St. Geol. Inst. of D. Štúr*, (archive no. AP4634), 171 pp.

Vozár, J., 1974: Stavba permských vulkanitov chočskej jednotky na severných svahoch Nízkych Tatier. *Západné Karpaty, séria Mineralógia, petrografia, geochémia, metalogenéza, ložiská*, 1, 7 – 49.

Vozár, J., Bujnovský, A., Vaškovský, I., Vozárová, A., Hanzel, V., Šucha, P., Lukáčik, E., Hanáček, J., Stankovič, J., Biely, A., Planderová, E. & Muška, P., 1983: Vysvetlivky na geologickej mape 1 : 25 000, list 36-221 (Malužiná-1). *Manuscript. Bratislava, Archive of St. Geol. Inst. of D. Štúr* (archive no. 57054), 122 pp.

Webb, J. A., 2021: Supergene sulphuric acid speleogenesis and the origin of hypogene caves: evidence from the Northern Pennines, UK. *Earth Surface Processes and Landforms*, 46, 2, 455 – 464. https://doi.org/10.1002/esp.5037.

Zoubek, V., 1952: Zpráva o výzkumu východní časti nízkotatranského jaderného pohoří. *Manuscript. Praha, Ústřední ústav geologický, Bratislava, Archive of St. Geol. Inst. of D. Štúr* (archive no. 3400), 20 pp.

# Geologické pomery a vznik Modrej jaskyne s modrými a zelenými sintrovými útvarmi (stredné Slovensko)

Modrá jaskyňa pri obci Malužiná je dosiaľ jedinou jaskyňou na Slovensku, v ktorej bol opísaný výskyt modrej a zelenej sintrovej výzdoby. Jaskyňa sa nachádza na severozápadných svahoch Nízkych Tatier na ľavom brehu toku Boca, v miestach, kde sa doň vlieva prítok Malužiná. Jaskyňa bola vytvorená v strednotriasových karbonátoch hronika. Zastupujú ich prevažne dolomity, v článku neformálne označované ako „čiernovážske karbonáty“. Prvotné analýzy jaskynnej výzdoby po jej objavení v roku 2016 ako príčinu zafarbenia sintrovej výzdoby určili prítomnosť medi. Za zdroj medi sa považovali produkty zvetrávania permských vulkanitov malužinského súvrstvia, konkrétne baritovo-sulfidové žilky, ktoré sa vyskytujú vo vulkanitoch. Sporadické zmienky o Pb-Zn-(Cu) mineralizácii prítomnej priamo v čiernovážskych karbonátoch nás však viedli k hľadaniu alternatívneho zdroja medi. Nadväzný rešeršný výskum v archíve Štátneho geologického ústavu Dionýza Štúra smeroval k objaveniu niekoľkých nepublikovaných manuskriptov. Tie sa pomerne rozsiahlo zaoberali zrudnením v okolí Modrej jaskyne a obsahovali pomerne rozsiahle údaje o Pb-Zn-(Cu) zrudnení čiernovážskych karbonátov. Správy o prieskume obsahujú údaje o mineralizácii v okolí baní v úžľabine zvanej Olovienka, prospekčných vrtoch Ma-1 a Ma-2 aj početných chemických a spektrálnych analýzach, ktoré sa realizovali v okolí jaskyne (obr. 1, 2 a 3). Tieto údaje museli nutne viesť k reinterpretácii pôvodných predstáv o zdroji medi.

Údaje z manuskriptov viedli k nutnosti preskúmať jaskyňu z geologického a geomorfologického hľadiska, ako aj nanovo zmapovať okolie jaskyne. Jaskyne vyskytujúce sa v karbonátoch obsahujúcich Pb-Zn zrudnenie môžu byť vytvárané kyselinou sírovou pochádzajúcou z oxidácie sulfidových rúd. Preto sa realizovalo detailné štúdium morfotvarov jaskyne, litológie materskej horniny jaskyne a jej štruktúrno-tektonického porušenia s cieľom objasniť pôvod jaskyne aj pôvod sfarbenia jej výzdoby. Použili sa metódy priameho terénneho výskumu aj nepriameho štúdia z 3D modelu jaskyne zostrojeného pomocou mobilného laserového terestrického skenera. Na geologických mapách z archívnych prác sa v okolí Modrej jaskyne nachádzalo viacero závažných nezhôd. Z nich vyplývali nejasnosti v tektonickej interpretácii hronika, ako aj nekonzistentnosť v distribúcii a rozsahu riečnych terás. Z týchto rozporov vyplynula nutnosť aspoň čiastočne reambulovať geologickú mapu v okolí Modrej jaskyne.

Na základe terénneho mapovania doplneného o digitalizované údaje z manuskriptov v okolí Modrej jaskyne interpretujeme existenciu dvoch príkrovov hronika. „Čiernovážske karbonáty“ tvoriace materskú horninu jaskyne budujú vrchnú časť spodného príkrovu, ktorá bola tektonicky imbrikovaná, a niektorí predchádzajúci autori ju považovali za tretí príkrov hronika. Táto deformovaná zóna sa vytvorila medzi dvomi rigidnejšími súbormi hornín – permskými vulkanitmi spodného príkrovu a hrubým telesom strednotriasových karbonátov vrchného príkrovu (obr. 1C, 2 a 4). Podotýkame, že tým nepopierame možnosť existencie troch (prípadne aj viacerých) príkrovov hronika mimo nami študovanej oblasti. Zdá sa, že Pb-Zn-(Cu) zrudnenie sa viaže na plochy prešmykov v imbrikovanej zóne. Príkrovová stavba hronika v oblasti je následne porušená mladšími zlomami, pričom jeden z týchto zlomov mohol narušiť kontinuitu pásu zrudnenia medzi baňami na Olovienke a Modrou jaskyňou (obr. 2A).

Mapovanie riečnych terás v okolí jaskyne bolo sťažené kolapsovými krasovými procesmi a antropogénnou modifikáciou reliéfu, ktoré zastierali pôvodnú morfológiu terás. Napriek tomu bolo možné vyčleniť tri skupiny terás, ktoré sme označili vrchné, stredné a spodné. Modrá jaskyňa bola vytvorená pod povrchom vrchných terás a väčšina jej priestorov sa vyskytuje medzi úrovňami vrchných až stredných terás, s výnimkou niektorých najnižšie položených priestorov. Na základe analógie s terasami Váhu v Liptovskej kotline sa vek vrchných terás (a súčasne vznikajúcej jaskyne) odhaduje na stredný pleistocén.

V jaskyni sú excelentne pozorovateľné geologické pomery jej materskej horniny, ktoré by prostredníctvom čisto povrchových terénnych prác nebolo možné identifikovať (obr. 5, 6 a 7). Severozápadná časť jaskyne je vytvorená vo vrstvovitých dolomitoch, zatiaľ čo v juhozápadnej časti jaskyne sú masívne dolomity a stýkajú sa na sv.-jz. zlome prebiehajúcom Malužinským dómikom. V Bocianskom baníckom dóme možno pozorovať výraznú vrásovo-násunovú štruktúru a v Malužinskom dómiku je viditeľný dextrálny sv.-jz. zlom segmentujú-

ci plocho uklonené prešmyky. Celkovo sme pozorovali štyri súbory strmých krehkých porúch ovplyvňujúcich priebeh jaskynných priestorov: sz.-jv. až ssz.-jjv., v.-z., ssv.-jjz. a sv.-jz. poruchy. Vek aktivity väčšiny porúch nebolo možné vymedziť, no v prípade vrásovo-násunovej štruktúry sa predpokladá aktivita v strednej časti kriedy. Na základe porovnania s paleonapäťovými štúdiami možno zároveň odhadnúť vek dextrálneho zlomu prebiehajúceho Malužinským dómikom na neskorý paleocén až stredný eocén. V jaskyni boli pozorované náteky malachitu a azuritu, ktoré sa vyskytovali na sv.-jz. až sz.-jv. poruchách. Výskyty zafarbených sintrových útvarov sa obmedzovali iba na sz.-jv. poruchy. V jednom prípade sa zdá, že azurit tvorí minerálny akrečný stupeň na dextrálnom zlome v Malužinskom dómiku, čo by umožňovalo presnejšie vekové zaradenie tejto sekundárnej mineralizácie. Vzhľadom na typický spôsob tvorby týchto minerálov v oxidačnej zóne sa však tieto minerály mohli tvoriť vo viacerých etapách, keď v študovanej oblasti dochádzalo k výzdvihu a denudácii horninových súborov. Možný časový diapazón tvorby malachitu a azuritu je teda pomerne široký – krieda až skorý eocén a od skorého miocénu po holocén. Predpokladá sa, že modro až zeleno sfarbené sintre sa začali tvoriť po vzniku jaskyne. Ich maximálny vek je teda stredný pleistocén, mnohé z nich však budú nepochybne aj mladšie.

Na základe morfologického štúdia možno konštatovať, že oxidácia sulfidov a tvorba kyseliny sírovej neboli hlavnými činiteľmi v genéze jaskyne. Napriek tomu existujú určité náznaky, že tieto procesy prispeli k zvýšeniu iniciálnej porozity dolomitov, ktorá neskôr uľahčila jej následnú tvorbu. Ide predovšetkým o blízku prítomnosť mineralizovanej zóny obsahujúcej sulfidové minerály vo vrte Ma-2, ako aj porézne dolomity a o hrdzavohnedé rezíduá v žilkách (azda po oxidácii sulfidov) pozorované vo vrte, na povrchu aj v jaskyni. Jaskyňa bola vytvorená agresívnou povrchovou vodou, ktorá prenikala do skalného masívu v troch hlavných štádiách. Jemnozrnný charakter sedimentov a absencia tvarov indikujúcich rýchle prúdenie vody naznačuje, že jaskyňa sa tvorila rozptýlene vnikajúcou pomaly tečúcou až stagnujúcou vodou. V prvom štádiu sa jaskyňa tvorila vo freatickej zóne (pod hladinou podzemnej vody) počas tvorby vrchných terás, pod ktorými sa nachádza. Svedčí o tom prítomnosť početných freatických foriem sledujúcich vrstvové plochy aj poruchy jaskyne. V druhej fáze, počas epizodického zarezávania doliny a tvorby stredných a spodných riečnych terás, prebiehala remodelácia jaskyne v epifreatickej zóne (t. j. pri hladine podzemnej vody). Jaskyňa bola vystavovaná opakovaným záplavám. Svedčí o tom prítomnosť epifreatickej modelácie skalných stien v niektorých častiach jaskyne. Stopy epizodického zaplavovania nesú na sebe aj zafarbené kvaple. To indikuje, že sa zrejme vytvorili v skorých štádiách druhej fázy vývoja jaskyne. Tretie štádium vývoja jaskyne je spojené s jej remodeláciou rútivými procesmi, ktoré sú najvýraznejšie v jej vstupných častiach, Bocianskom baníckom dóme a Malužinskom dómiku.

Tento článok podčiarkuje význam jaskýň v geológii ako „prirodzených vrtov“, značne uľahčujúcich štúdium geologických pomerov, obzvlášť v horšie odkrytých oblastiach.

Doručené / Recieved: 14. 7. 2025
Prijaté na publikovanie / Accepted: 1. 9. 2025

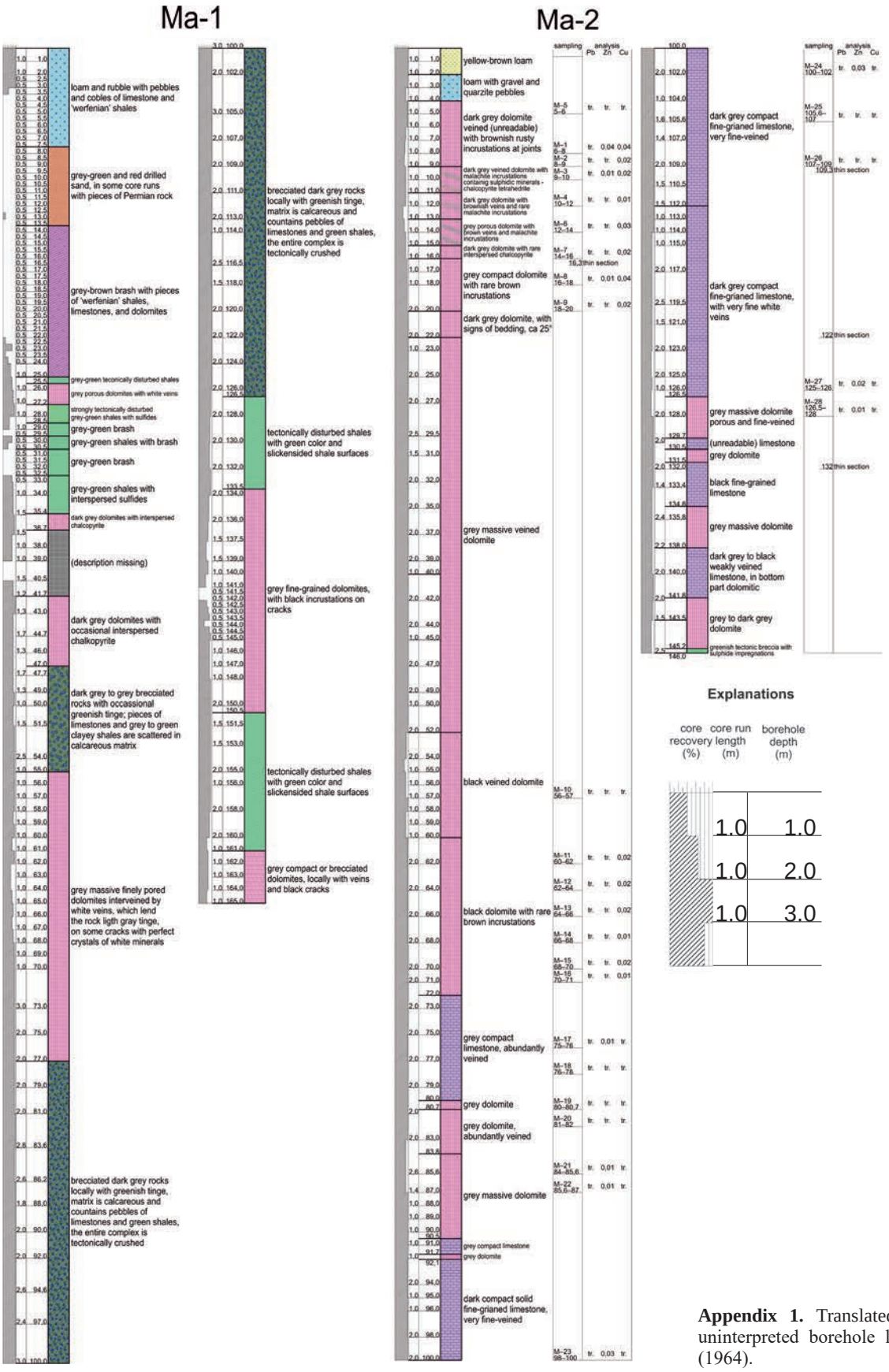


**Appendix 1.** Translated and coloured uninterpreted borehole logs from Biely (1964).

**Appendix 2.** A table of the samples with their Pb, Zn, and Cu contents determined by a chemical analysis from Hanáček (1963). The WGS coordinates were determined by georeferencing the author's map. The values are percentual.

| Sample id | X | Y | Pb [%] | Zn [%] | Cu [%] | Lithological description |
|---|---|---|---|---|---|---|
| 1 | 48,9842817 | 19,7641870 | | 0,02 | | grey to dark grey fine crystalline thin-bedded to bedd dolomites, permeated by an irregular network of fractures |
| 2 | 48,9842774 | 19,7641744 | 0,55 | 0,06 | | grey to dark grey fine crystalline thin-bedded to bedd dolomites, permeated by an irregular network of fractures |
| 3 | 48,9842733 | 19,7641575 | 0,55 | 0,03 | | grey to dark grey fine crystalline thin-bedded to bedd dolomites, permeated by an irregular network of fractures |
| 4 | 48,9842682 | 19,7641412 | 0,13 | 0,02 | | grey to dark grey fine crystalline thin-bedded to bedd dolomites, permeated by an irregular network of fractures |
| 5 | 48,9842630 | 19,7641254 | 0,45 | 0,61 | | grey to dark grey fine crystalline thin-bedded to bedd dolomites, permeated by an irregular network of fractures |
| 6 | 48,9842588 | 19,7641091 | 0,05 | 0,13 | | grey to dark grey fine crystalline thin-bedded to bedd dolomites, permeated by an irregular network of fractures |
| 7 | 48,9842558 | 19,7640924 | 0,05 | 0,05 | | grey to dark grey fine crystalline thin-bedded to bedd dolomites, permeated by an irregular network of fractures |
| 8 | 48,9842503 | 19,7640785 | 0,15 | 0,24 | | grey to dark grey fine crystalline thin-bedded to bedd dolomites, permeated by an irregular network of fractures |
| 9 | 48,9842662 | 19,7641929 | 0,21 | 0,16 | | grey to dark grey fine crystalline thin-bedded to bedd dolomites, permeated by an irregular network of fractures |
| 11 | 48,9842584 | 19,7641730 | 1,57 | 1,53 | 0,04 | grey to dark grey fine crystalline thin-bedded to bedd dolomites, permeated by an irregular network of fractures |
| 12 | 48,9842504 | 19,7641527 | 0,27 | 0,75 | 0,01 | grey to dark grey fine crystalline thin-bedded to bedd dolomites, permeated by an irregular network of fractures |
| 13 | 48,9818605 | 19,7694132 | | 0,06 | | dark grey dolomites |
| 14 | 48,9814303 | 19,7709837 | | 0,05 | | grey limestones |
| 15 | 48,9814892 | 19,7711366 | | 0,04 | | grey dolomites |
| 16 | 48,9815505 | 19,7715276 | | 0,04 | | grey dolomites |
| 17 | 48,9813546 | 19,7714617 | | 0,01 | | grey dolomites |
| 18 | 48,9811902 | 19,7713805 | | 0,01 | | grey dolomites |
| 19 | 48,9809951 | 19,7713329 | | 0,01 | | grey dolomites |
| 20 | 48,9808454 | 19,7713113 | | | | grey dolomites |
| 21 | 48,9846194 | 19,7640968 | | | | grey limestones |
| 22 | 48,9845866 | 19,7644514 | | | | grey limestones with calcite veins |
| 23 | 48,9845362 | 19,7649086 | | | | grey limestones with calcite veins |
| 25 | 48,9844229 | 19,7632567 | | | | light grey dolomites |
| 27 | 48,9844965 | 19,7632370 | | | | light grey dolomites |
| 28 | 48,9844204 | 19,7635227 | | 0,03 | | light grey dolomites |
| 30 | 48,9842301 | 19,7627308 | | 0,02 | 0,03 | dark grey dolomites |
| 31 | 48,9841557 | 19,7628238 | | 0,05 | 0,03 | grey dolomites |
| 32 | 48,9837842 | 19,7613583 | | | | dark grey brecciated dolomites |
| 33 | 48,9835861 | 19,7610575 | | | | grey dolomites |
| 34 | 48,9837424 | 19,7615061 | | | | grey crystalline dolomites |
| 35 | 48,9836759 | 19,7616411 | | | | grey crystalline dolomites |
| 36 | 48,9770855 | 19,7773092 | | | | original description missing |

**Appendix 2** – continued

| Sample id | X | Y | Pb [%] | Zn [%] | Cu [%] | Lithological description |
|---|---|---|---|---|---|---|
| 37 | 48,9767451 | 19,7768792 | | | | original description missing |
| 38 | 48,9772684 | 19,7768938 | | | 0,05 | original description missing |
| 39 | 48,9775010 | 19,7766933 | | | 0,04 | original description missing |
| 40 | 48,9774078 | 19,7763300 | | | 0,05 | original description missing |
| 41 | 48,9775575 | 19,7762142 | | | 0,02 | original description missing |
| 42 | 48,9781897 | 19,7730017 | | | | original description missing |
| 44 | 48,9864362 | 19,7638497 | | | | light grey limestones |
| 45 | 48,9864973 | 19,7640513 | 0,2 | | | light grey dolomites |
| 55 | 48,9748475 | 19,7387252 | | 0,02 | | grey limestones with calcite veins – tallus |
| 56 | 48,9746112 | 19,7380887 | | 0,01 | | light grey dolomites – tallus |
| 57 | 48,9748806 | 19,7381881 | | 0,02 | | grey, dark grey massive limestones – rocky outcrop |
| 58 | 48,9749682 | 19,7376409 | | 0,26 | | grey, dark grey massive limestones – rocky outcrop |
| 64 | 48,9733406 | 19,7337661 | | | | grey massive limestones |
| 65 | 48,9730303 | 19,7339559 | | 0,02 | | dark grey massive limestones |
| 66 | 48,9728781 | 19,7333380 | | | | dark grey massive limestones |
| 67 | 48,9721530 | 19,7262554 | | | | dark grey massive limestones |
| 68 | 48,9718235 | 19,7254656 | | 0,01 | | dark grey massive limestones |
| 69 | 48,9725048 | 19,7261293 | | 0,01 | | dark grey limestones |
| 72 | 48,9709709 | 19,7204362 | | 0,03 | | grey bedded limestones |
| 74 | 48,9710796 | 19,7213818 | | 0,03 | | grey massive limestones |
| 75 | 48,9704967 | 19,7225164 | | | | grey surcose dolomites – tallus |
| 76 | 48,9707827 | 19,7229262 | | | | grey surcose dolomites – tallus |
| 84 | 48,9765499 | 19,7465192 | | | | dark grey bedded limestones |
| 89 | 48,9693474 | 19,7142686 | | 0,01 | | grey massive dolomites – outcrop |
| 90 | 48,9830397 | 19,7698286 | | | | grey massive dolomites – outcrop |
| 91 | 48,9705224 | 19,7185005 | | | | grey limestones |
| 92 | 48,9685994 | 19,7116217 | | | | grey dolomitic limestones |
| 114 | 48,9791450 | 19,7712074 | | | | grey dolomites |
| 115 | 48,9790837 | 19,7724781 | | | | grey dolomites |
| 116 | 48,9790363 | 19,7731426 | | | | dark grey dolomites |
| 120 | 48,9779315 | 19,7728199 | | | | original description missing |
| 121 | 48,9775792 | 19,7728553 | | | | original description missing |
| 122 | 48,9770272 | 19,7728670 | | | | original description missing |
| 123 | 48,9763835 | 19,7728413 | | | | original description missing |
| 124 | 48,9755806 | 19,7729462 | | | | original description missing |
| 125 | 48,9780151 | 19,7734468 | | | | original description missing |
| 126 | 48,9776141 | 19,7743270 | | | | original description missing |
| 132 | 48,9759709 | 19,7801822 | | | | original description missing |

**Appendix 3.** A table of the samples with their trace element contents determined by a spectral analysis from Hanáček (1963). The WGS coordinates were determined by georeferencing the author's map.

| Sample id | X | Y | Ca | Mg | Fe | Si | Al | Mn | Sr | Na | K | Li | Ti | Pb | Zn | Cu | Ag | Bi | Ni | Co | Cr | Ba | V | B | Zr | Cd |
|---|---|---|---|---|---|---|---|---|---|---|---|---|---|---|---|---|---|---|---|---|---|---|---|---|---|---|
| 1 | 48,9842817 | 19,7641870 | 6 | 3 | 2 | 3 | 2 | 1 | 3 | 2 | | 1 | | 1 | 0 | 1 | 1 | | | | 1 | 1 | | | | |
| 3 | 48,9842733 | 19,7641575 | 6 | 6 | 5 | 3 | 2 | 4 | 2 | 2 | | 1 | 2 | 3 | 3 | 1 | 1 | | 2 | 2 | 1 | 1 | | | | |
| 6 | 48,9842588 | 19,7641091 | 6 | 6 | 4 | 3 | 3 | 4 | 2 | 2 | | 1 | 2 | 2 | 3 | 1 | 1 | | | | 1 | 1 | | | | |
| 8 | 48,9842503 | 19,7640785 | 6 | 6 | 4 | 3 | 2 | 4 | 2 | 2 | | 1 | 2 | 3 | 4 | 1 | 1 | | | | 1 | 1 | | | | |
| 9 | 48,9842662 | 19,7641929 | 6 | 6 | 4 | 3 | 2 | 4 | 2 | 2 | | 1 | 2 | 3 | 4 | 1 | 1 | | | | 1 | 1 | | | | |
| 11 | 48,9842584 | 19,7641730 | 6 | 6 | 3 | 3 | 2 | 4 | 2 | 2 | | 1 | | 4 | 4 | 1 | 2 | | | | 1 | 1 | | | | 2 |
| 13 | 48,9818605 | 19,7694132 | 6 | 6 | 2 | 3 | 2 | 3 | 2 | 2 | | 1 | 2 | 2 | 2 | 1 | 1 | | | | 1 | 1 | | | | |
| 14 | 48,9814303 | 19,7709837 | 6 | 3 | 2 | 3 | 3 | 2 | 3 | 2 | | 1 | | 1 | 0 | 1 | | | | | | 1 | | | | |
| 16 | 48,9815505 | 19,7715276 | 6 | 6 | 3 | 3 | 3 | 3 | 2 | 2 | | 1 | 2 | 2 | 2 | 1 | | | 1 | | 1 | 1 | | | | |
| 18 | 48,9811902 | 19,7713805 | 6 | 6 | 3 | 3 | 2 | 3 | 2 | 2 | | 1 | | 0 | 0 | 1 | 1 | | 1 | | 1 | 1 | | | | |
| 21 | 48,9846194 | 19,7640968 | 6 | 5 | 3 | 4 | 4 | 2 | 3 | 3 | | 1 | | 2 | 0 | 2 | 1 | | | | 1 | 2 | | | | |
| 22 | 48,9845866 | 19,7644514 | 6 | 5 | 3 | 4 | 3 | 2 | 3 | 3 | | | | 1 | 0 | 2 | | | 1 | | 1 | 2 | | | | |
| 23 | 48,9845362 | 19,7649086 | 6 | 3 | 2 | 3 | 2 | 1 | 3 | 2 | | 1 | | 1 | 0 | 1 | 1 | | | | 1 | 1 | | | | |
| 24 | 48,9846270 | 19,7625666 | 5 | 6 | 2 | 3 | 2 | 2 | 2 | 3 | | 1 | | 2 | 0 | 2 | | | | | 1 | 2 | | | | |
| 25 | 48,9844229 | 19,7632567 | 6 | 6 | 2 | 3 | 3 | 2 | 2 | 2 | | 1 | | 2 | 0 | 2 | | | 1 | | 1 | 1 | | | | |
| 30 | 48,9842301 | 19,7627308 | 6 | 6 | 3 | 3 | 3 | 3 | 3 | 2 | | 1 | | 1 | 2 | 1 | 1 | | | | 1 | 1 | | | | |
| 32 | 48,9837842 | 19,7613583 | 6 | 6 | 5 | 4 | 3 | 4 | 2 | 2 | | 1 | | 1 | 0 | 2 | 1 | | 1 | | 1 | 3 | | | | |
| 33 | 48,9835861 | 19,7610575 | 6 | 6 | 5 | 4 | 4 | 3 | 2 | 2 | 3 | 2 | 2 | 0 | 0 | 1 | 1 | | 1 | | 1 | 3 | | | | |
| 34 | 48,9837424 | 19,7615061 | 6 | 6 | 5 | 4 | 2 | 4 | 3 | 2 | 3 | 2 | | 0 | 0 | 1 | | | 1 | | 1 | 2 | | | | |
| 35 | 48,9836759 | 19,7616411 | 6 | 6 | 5 | 4 | 3 | 3 | 3 | 3 | 3 | 2 | | 1 | 0 | 2 | 1 | | 1 | | 1 | 2 | 2 | 2 | | |
| 36 | 48,9770855 | 19,7773092 | 6 | 6 | 4 | 4 | 3 | 3 | 3 | 3 | | 1 | | 0 | 0 | 3 | 1 | | | | 1 | 2 | | | | |
| 37 | 48,9767451 | 19,7768792 | 6 | 6 | 5 | 4 | 4 | 4 | 4 | 3 | 3 | 2 | 2 | 1 | 3 | 0 | 1 | | | | 2 | 3 | | | | |
| 38 | 48,9772684 | 19,7768938 | 6 | 6 | 5 | 3 | 4 | 4 | 4 | 2 | | 1 | | 1 | 0 | 0 | 1 | 2 | | | 1 | 2 | | | | |
| 39 | 48,9775010 | 19,7766933 | 6 | 6 | 3 | 3 | 4 | 4 | 4 | 2 | | 1 | | 1 | 0 | 0 | 1 | | | | 1 | 2 | | | | |
| 40 | 48,9774078 | 19,7763300 | 6 | 6 | 2 | 3 | 2 | 3 | 3 | 2 | | 1 | | 0 | 0 | 1 | | | 1 | | 1 | 2 | | | | |

**Appendix 3 –** continued

| Sample id | X | Y | Ca | Mg | Fe | Si | Al | Mn | Sr | Na | K | Li | Ti | Pb | Zn | Cu | Ag | Bi | Ni | Co | Cr | Ba | V | B | Zr | Cd |
|---|---|---|---|---|---|---|---|---|---|---|---|---|---|---|---|---|---|---|---|---|---|---|---|---|---|---|
| 41 | 48,9775575 | 19,7762142 | 6 | 6 | 4 | 3 | 2 | 3 | 2 | 2 | | 1 | | 1 | 0 | 2 | 1 | | | | 1 | 1 | | | | |
| 42 | 48,9781897 | 19,7730017 | 6 | 6 | 4 | 4 | 2 | 4 | 3 | 2 | | 1 | | 2 | 0 | 2 | 1 | | 1 | | 1 | 2 | | | | |
| 44 | 48,9864362 | 19,7638497 | 6 | 3 | 2 | 3 | 3 | 1 | 3 | 2 | 2 | 1 | | 0 | 0 | 1 | | | 1 | | 2 | 1 | | | | |
| 55 | 48,9748475 | 19,7387252 | 6 | 5 | 3 | 4 | 3 | 4 | 3 | 2 | | 1 | | 2 | 0 | 2 | 1 | 2 | 1 | | 1 | 2 | 2 | | | |
| 56 | 48,9746112 | 19,7380887 | 6 | 6 | 3 | 4 | 5 | 3 | 2 | 3 | | 1 | 2 | 3 | 0 | 2 | 1 | | 2 | | 1 | 0 | 2 | | | |
| 57 | 48,9748806 | 19,7381881 | 6 | 6 | 3 | 3 | 2 | 4 | 3 | 2 | | 1 | | 3 | 0 | 1 | | | | | 1 | 2 | | | | |
| 60 | 48,9758495 | 19,7372622 | 6 | 5 | 3 | 4 | 5 | 3 | | 2 | 3 | 1 | 2 | 1 | 0 | 0 | | | | | 1 | 4 | | | | |
| 61 | 48,9762772 | 19,7372370 | 6 | 5 | 3 | 4 | 3 | 2 | 4 | 3 | 3 | 1 | | 2 | 0 | 2 | 1 | | | | 1 | 2 | | | | |
| 63 | 48,9744988 | 19,7330155 | 6 | 5 | 3 | 3 | 3 | 3 | 4 | 2 | | 1 | | 2 | 0 | 0 | 1 | | | | 1 | 2 | | | | |
| 64 | 48,9733406 | 19,7337661 | 6 | 4 | 2 | 3 | 3 | 3 | 4 | 2 | | 1 | | 2 | 0 | 0 | 1 | | | | | 2 | | | | |
| 65 | 48,9730303 | 19,7339559 | 6 | 5 | 3 | 3 | 3 | 3 | 4 | 3 | | 1 | | 2 | 3 | 0 | 2 | 2 | 2 | | 2 | 2 | | | | |
| 66 | 48,9728781 | 19,7333380 | 6 | 4 | 2 | 3 | 3 | 3 | 3 | 2 | | 1 | | 2 | 3 | 1 | 1 | | | | 1 | 2 | | | | |
| 67 | 48,9721530 | 19,7262554 | 6 | 6 | 3 | 4 | 3 | 3 | 3 | 2 | | 1 | | 2 | 3 | 2 | | | | | 1 | 2 | | | | |
| 68 | 48,9718235 | 19,7254656 | 6 | 6 | 4 | 4 | 3 | 4 | 3 | 2 | | 1 | | 1 | 3 | 2 | 1 | | | | 1 | 2 | | | | |
| 69 | 48,9725048 | 19,7261293 | 6 | 5 | 2 | 4 | 3 | 3 | 4 | 3 | | 1 | | 1 | 0 | 2 | 1 | | | | 1 | 2 | | | | |
| 70 | 48,9740197 | 19,7213344 | 6 | 5 | 3 | 4 | 5 | 3 | | 3 | 3 | 1 | 2 | 1 | 0 | 0 | 1 | 2 | | | 1 | 2 | | | | |
| 71 | 48,9701209 | 19,7218263 | 6 | 4 | 2 | 3 | 3 | 3 | 3 | 2 | | 1 | | 2 | 3 | 3 | | | | | 1 | 2 | | | | |
| 72 | 48,9709709 | 19,7204362 | 6 | 5 | 2 | 4 | 3 | 3 | | 2 | | 1 | | 1 | 0 | 3 | | | | | 1 | 2 | | | | |
| 73 | 48,9711811 | 19,7230802 | 6 | 5 | 3 | 4 | 3 | 3 | 2 | 2 | | 1 | | 2 | 3 | 1 | | 2 | | | 1 | 2 | | | | |
| 74 | 48,9710796 | 19,7213818 | 6 | 6 | 2 | 3 | 3 | 3 | 3 | 2 | | 1 | | 2 | 3 | 1 | 1 | | | | 1 | 2 | | | | |
| 75 | 48,9704967 | 19,7225164 | 6 | 6 | 2 | 4 | 3 | 4 | 2 | 2 | | 1 | | 0 | 0 | 1 | | | | | 2 | 2 | | | | |
| 76 | 48,9707827 | 19,7229262 | 6 | 3 | 3 | 4 | 3 | 3 | 4 | 2 | 3 | 2 | | 0 | 3 | 0 | | | | | 1 | 2 | | | | |
| 77 | 48,9714196 | 19,7241371 | | 6 | 3 | 4 | 3 | 4 | 3 | 2 | | 1 | | 0 | 0 | 2 | | | 2 | | | 1 | 2 | | | |
| 78 | 48,9713251 | 19,7205325 | 6 | 6 | 2 | 4 | 3 | 3 | 3 | 2 | | 1 | | 1 | 0 | 1 | 1 | | 1 | | 1 | 2 | | | | |
| 80 | 48,9695588 | 19,7142018 | | 4 | 2 | 3 | 3 | 4 | 4 | 2 | | 1 | | 2 | 3 | 1 | | | | | 1 | 2 | | | | |

**Appendix 3 –** continued

| Sample id | X | Y | Ca | Mg | Fe | Si | Al | Mn | Sr | Na | K | Li | Ti | Pb | Zn | Cu | Ag | Bi | Ni | Co | Cr | Ba | V | B | Zr | Cd |
|---|---|---|---|---|---|---|---|---|---|---|---|---|---|---|---|---|---|---|---|---|---|---|---|---|---|---|
| 81 | 48,9778625 | 19,7442604 | 6 | 5 | 3 | 4 | 3 | 4 | 4 | 2 | 3 | 1 | | 0 | 0 | 0 | | 2 | | | 1 | 2 | | | | |
| 83 | 48,9764859 | 19,7460100 | 6 | 4 | 2 | 3 | 2 | 4 | 3 | 2 | | 1 | | 2 | 0 | 1 | | | | | 1 | 2 | | | | |
| 84 | 48,9765499 | 19,7465192 | 6 | 4 | 2 | 4 | 3 | 4 | 3 | 2 | | 1 | | 2 | 0 | 2 | | | | | 1 | 2 | | | | |
| 85 | 48,9775099 | 19,7477704 | | 6 | 3 | 4 | 3 | 4 | 3 | 2 | | 1 | | 2 | 0 | 1 | | | | | 1 | 2 | | | | |
| 86 | 48,9772344 | 19,7477348 | | 6 | 3 | 4 | 3 | 4 | 3 | 2 | | 1 | | 2 | 3 | 1 | | | | | 1 | 2 | | | | |
| 87 | 48,9778560 | 19,7494183 | | 4 | 2 | 3 | 3 | 4 | 4 | 2 | | 1 | | 2 | 0 | 1 | 1 | | | | 2 | 2 | | | | |
| 89 | 48,9693474 | 19,7142686 | | 6 | 3 | 4 | 3 | 3 | 3 | 2 | | 2 | 2 | 3 | 3 | 1 | 1 | | | | 1 | 2 | | | | |
| 90 | 48,9830397 | 19,7698286 | | 6 | 3 | 3 | 3 | 4 | 3 | 2 | | 1 | | 2 | 0 | 2 | | | | | 1 | 2 | | | | |
| 91 | 48,9705224 | 19,7185005 | 6 | 5 | 2 | 3 | 3 | 3 | 4 | 2 | | 1 | | 2 | 0 | 2 | | | | | 1 | 2 | | | | |
| 92 | 48,9685994 | 19,7116217 | | 4 | 2 | 3 | 3 | 2 | 4 | 2 | | 1 | | 1 | 0 | 0 | | | | | 1 | 2 | | | | |
| 94 | 48,9828501 | 19,7696596 | 6 | 5 | 3 | 4 | 4 | 3 | 4 | 2 | | 1 | | 2 | 3 | 1 | 1 | | | | 1 | 2 | | | | |
| 95 | 48,9821864 | 19,7685473 | 6 | 6 | 2 | 3 | 3 | 3 | 3 | 2 | | 1 | 2 | 1 | 3 | 1 | 1 | | | | 1 | 2 | | | | |
| 95a | 48,9821864 | 19,7685473 | 6 | 6 | 2 | 3 | 3 | 4 | 3 | 2 | | 1 | | 1 | 0 | 2 | | | 1 | | 1 | 1 | 2 | | | |
| 96 | 48,9797186 | 19,7601149 | 6 | 6 | 2 | 3 | 2 | 4 | 3 | 2 | | 1 | | 2 | 0 | 1 | | | | | 1 | 2 | | | | |
| 97 | 48,9811184 | 19,7598472 | 6 | 5 | 5 | 4 | 3 | 4 | 2 | 2 | | 1 | 2 | 1 | 0 | 2 | 1 | | 2 | | 1 | 1 | | | | |
| 98 | 48,9816359 | 19,7598312 | 6 | 6 | 4 | 4 | 2 | 4 | 3 | 2 | | 1 | | 2 | 0 | 2 | 1 | | 2 | | 2 | 2 | | | | |
| 99 | 48,9835240 | 19,7594047 | 6 | 6 | 3 | 3 | 3 | 3 | 3 | 2 | | 1 | | 1 | 0 | 1 | | | 1 | | 1 | 1 | | | | |
| 100 | 48,9790915 | 19,7632550 | 6 | 6 | 3 | 4 | 3 | 3 | 2 | 3 | | 1 | | 2 | 0 | 2 | 1 | | | | 1 | 0 | | | | |
| 103 | 48,9831684 | 19,7661290 | 6 | 6 | 5 | 4 | 3 | 4 | 2 | 2 | | 1 | | 1 | 0 | 2 | 1 | | 1 | | 1 | 1 | | | | |
| 105 | 48,9835962 | 19,7664490 | 6 | 6 | 3 | 3 | 3 | 2 | 2 | 2 | | 1 | | 0 | 0 | 1 | | | 2 | | 2 | 1 | | | | |
| 108 | 48,9819677 | 19,7681906 | 6 | 6 | 3 | 3 | 3 | 4 | 2 | 3 | | 1 | 2 | 2 | 0 | 0 | 1 | | 1 | | 1 | 2 | | | | |
| 109 | 48,9825183 | 19,7683925 | 6 | 5 | 3 | 4 | 3 | 3 | 3 | 2 | | 1 | | 2 | 3 | 2 | 1 | | | | | 1 | | | | |
| 110 | 48,9829824 | 19,7690261 | 6 | 5 | 3 | 4 | 3 | 2 | 3 | 2 | | 1 | | 2 | 3 | 1 | 1 | | | | 1 | 1 | | | | |
| 111 | 48,9815768 | 19,7707909 | 6 | 5 | 2 | 4 | 2 | 3 | 4 | 3 | | 1 | | 2 | 0 | 2 | 1 | | | | 1 | 2 | | | | |
| 112 | 48,9818031 | 19,7691618 | 6 | 6 | 3 | 4 | 3 | 4 | 3 | 2 | | 1 | | 2 | 0 | 2 | 1 | | 1 | | 1 | 2 | | 2 | | |

**Appendix 3 –** continued

| Sample id | X | Y | Ca | Mg | Fe | Si | Al | Mn | Sr | Na | K | Li | Ti | Pb | Zn | Cu | Ag | Bi | Ni | Co | Cr | Ba | V | B | Zr | Cd |
|---|---|---|---|---|---|---|---|---|---|---|---|---|---|---|---|---|---|---|---|---|---|---|---|---|---|---|
| 114 | 48,9791450 | 19,7712074 | 6 | 5 | 3 | 3 | 3 | 3 | 3 | 2 | | 1 | | 2 | 3 | 2 | 1 | | | | 1 | 2 | | | | |
| 115 | 48,9790837 | 19,7724781 | 6 | 6 | 5 | 4 | 4 | 4 | 3 | 2 | | 1 | | 1 | 0 | 3 | | 2 | 1 | | 1 | 2 | 2 | | | |
| 116 | 48,9790363 | 19,7731426 | 6 | 6 | 5 | 4 | 3 | 4 | 2 | 2 | | 2 | | 1 | 0 | 3 | 1 | | 1 | 2 | 1 | 2 | | | | |
| 120 | 48,9779315 | 19,7728199 | 6 | 6 | 3 | 4 | 3 | 4 | 2 | 2 | | 1 | | 1 | 0 | 2 | 1 | | 1 | | 1 | 1 | 2 | | | |
| 121 | 48,9775792 | 19,7728553 | 6 | 6 | 3 | 3 | 3 | 4 | | 3 | | 1 | 2 | 2 | 0 | 0 | 1 | | 1 | | 1 | 2 | | | | |
| 122 | 48,9770272 | 19,7728670 | 6 | 6 | 5 | 4 | 3 | 4 | 2 | 2 | | 1 | 2 | 1 | 0 | 2 | 1 | | 2 | | 1 | 1 | | | | |
| 123 | 48,9763835 | 19,7728413 | 6 | 6 | 4 | 4 | 3 | 4 | 2 | 2 | | 1 | | 2 | 0 | 2 | | | 1 | | 1 | 1 | 2 | | | |
| 124 | 48,9755806 | 19,7729462 | 6 | 6 | 3 | 4 | 4 | 3 | 2 | 3 | | 1 | | 1 | 0 | 2 | | | 1 | | 1 | 0 | | | | |
| 126 | 48,9776141 | 19,7743270 | 6 | 6 | 4 | 3 | 3 | 4 | 2 | 2 | | 1 | | 1 | 0 | 3 | 1 | | 1 | | 1 | 1 | | | | |
| 127 | 48,9774122 | 19,7750863 | 6 | 6 | 5 | 4 | 3 | 4 | 3 | 2 | | 1 | | 0 | 0 | 2 | | | | | 1 | 2 | 2 | | | |
| 129 | 48,9752718 | 19,7761723 | 6 | 6 | 5 | 4 | 4 | 4 | 3 | 2 | | 2 | | 1 | 0 | 2 | | 2 | 1 | | 1 | 2 | | | | |
| 131 | 48,9747114 | 19,7802218 | 6 | 5 | 2 | 4 | 3 | 3 | 3 | 2 | | | | 1 | 0 | 1 | | | | | 1 | 2 | | | | |
| 132 | 48,9759709 | 19,7801822 | 6 | 6 | 5 | 4 | 4 | 4 | 3 | 2 | | 2 | | 1 | 0 | 2 | 1 | 2 | 1 | | 1 | 2 | | | | |
| 139 | 48,9841158 | 19,7610114 | 6 | 6 | 5 | 5 | 5 | 4 | | 4 | 5 | 3 | 3 | 1 | 0 | 0 | 1 | | 2 | 2 | 2 | 3 | 2 | 2 | 2 | |
| 140 | 48,9842901 | 19,7609538 | 6 | 6 | 3 | 3 | 3 | 2 | 3 | 2 | | 1 | | 1 | 0 | 2 | | | 2 | | 1 | 1 | | | | |
| 141 | 48,9826885 | 19,7594937 | 6 | 6 | 4 | 4 | 4 | 4 | 2 | | | 1 | 2 | 2 | 3 | 0 | | | 2 | | 2 | 2 | | | | |
| 144 | 48,9743489 | 19,7805060 | 6 | 6 | 3 | 4 | 3 | 3 | 2 | 2 | | 1 | 2 | 2 | 0 | 1 | | | | | 1 | 1 | 2 | | | |

The explanation of the values denoted by numbers:
**6:** 1 000 000–100 000 ppm
**5:** 100 000–10 000 ppm
**4:** 10 000–1 000 ppm
**3:** 1 000–100 ppm
**2:** 1 000–10 ppm
**1:** 100–1 ppm